A Thesis for the Degree of Master of Engineering

# Antenna 3D Radiation Pattern Estimation in a Reverberation Environment

By

Cesar Whesly Segura

School of Mechanical and Aerospace Engineering

Graduate School

GYEONGSANG NATIONAL UNIVERSITY

August, 2017

# Antenna 3D Radiation Pattern Estimation in a Reverberation Environment

A Dissertation Submitted to the Faculty of the Graduate School of the Gyeongsang National University

By Cesar Whesly Segura

In partial fulfillment of the requirements

for the degree

of Master of Engineering

August, 2017

Dr. Koh Jinhwan, Dissertation Supervisor

**Approved by the committees of the Graduate School of Gyeongsang National University in partial fulfillment of the requirements for the degree of Master of Engineering**

**Dissertation Committee** _____

Chairperson

_____

_____

(Name and Signature)

Date: 2017. 07 . 20 .

**School of Mechanical and Aerospace Engineering**

**GRADUATE SCHOOL**

**GYEONGSANG NATIONAL UNIVERSITY**

# ACKNOWLEDGEMENT

The present work has been accomplished through the guidance of my advisor and collaboration between the members of the Adaptive Wireless Communication (AWC) laboratory. The constant flow of ideas and several trials to model and simulate structures in a software or implement algorithms have provided worth and quality to this work.

I thank my advisor, Prof. Koh Jinhwan, for his support when I chose this topic, for his guidance during development. Specially, for providing an environment in which researchers have broad options to study, review and propose their own study topics.

I want to thank the members of my laboratory who have helped me through my master studies to adapt in a new city, new environment, have taught me about their work and culture of their country.

In addition, I would like to thank to the School of Mechanical and Aerospace Engineering for the quality of education which have provided me with tools for a successfully completion of the work and their support in registration of courses and procedures in Gyeongsang National University, GNU.

Finally, I deeply thank my family who have motivated during these two years to show the best of myself in my work. My father, mother and sister are irreplaceable in my life and have granted me the strength to come to South Korea and achieve my dreams.

# CONTENTS

## FIGURE CONTENTS

## LIST OF TABLES

## SYMBOL DESCRIPTION

$G_D(\theta,\varphi)$: Antenna radiation pattern where $\theta$ and $\varphi$ stand for azimuth and elevation orientation.

$E(\theta,\varphi)$: Antenna electric far-field.

$R(\theta,\varphi)$: Auto-correlation function.

$\widehat{A}(\theta,\varphi)|_{f=f_0}$: Reverberation environment response when AUT does not possess pencil beam radiation pattern at frequency $f_0$.

$A(\theta,\varphi)|_{f=f0}$: Environment response when AUT possesses pencil-beam radiation pattern at frequency $f_0$.

$A(\theta,\varphi)_{t=t0}$: Environment response when AUT possesses pencil beam radiation pattern in time $t_0$.

$P_{reverberation}(\theta,\varphi)|_{f=f0}$: AUT measurement in reverberation environment at frequency $f_0$.

$P_{reververation}(\theta,\varphi)_{t=t_0}$ : AUT measurement in the reverberation environment at time $t_0$.

$P_{free-space}(\theta,\varphi)|_{f=f0}$: AUT free-space radiation pattern estimation at frequency $f_0$.

$P_{free-space}(\theta,\varphi)|_{t=t_0}$ : AUT free-space measurement at time $t_0$ , $P_{reververation}(\theta,\varphi)_{t=t_0}$ is AUT measurement in the reverberating environment at time $t_0$.

$H_{mn}(f)$: Channel Matrix transfer function.

$Y_m(f)$: AUT free-space radiation pattern measurement in TRM in frequency domain.

$S_n(f)$: AUT free-space radiation pattern measurement in VPA in frequency domain.

$\hat{S}_n(f)$: AUT free-space radiation pattern estimation in VPA in frequency domain.

$\alpha_m$: Weight vector for the Channel Matrix.

## ABSTRACT

Antenna 3D Radiation Pattern Estimation in a Reverberation Environment

Cesar Whesly

Dept. of Aerospace and Computer Systems Engineering

Graduate School, Gyeongsang National University

Advised by Professor

Koh Jinhwan

Impulse Response with 3D algorithm is a novel antenna free-space radiation pattern estimation technique in magnitude and phase. Impulse Response with 3D features deconvolution in azimuth and elevation angular domains to enhance quality of the antenna radiation pattern estimations with respect to the Impulse Response with 2D algorithm, a previous antenna free-space radiation pattern estimation technique. The antenna configuration system of Impulse Response technique has the following elements: Antenna Under Test (AUT) and probe antenna surrounded by metallic objects with finite conductivity. Metallic objects amplify reflections, diffractions and scatterings which interfere with AUT transmitted signal. A qualitative and quantitative comparison between Impulse Response with 3D and Impulse Response with 2D algorithms is established through contour graphs, magnitude and phase pattern graphs, and

quantifiers. Benefits of the proposed 3D free-space radiation pattern estimation technique are single frequency characterization and reuse of 3D Impulse Response of the Environment.

Time Reversal algorithm is an antenna free-space radiation pattern estimation technique featured in a reverberation environment facility defined as Time Reversal Electromagnetic Chamber (TREC). Elements of TREC are Antenna Under Test (AUT), Virtual Probe Array (VPA) and Time Reversal Mirror Antenna (TRM), all surrounded by metallic objects with finite conductivity. In the TREC, the AUT produces the excitation signal and transmits it as an electromagnetic wave, VPA samples the signal in each of its probe antennas. Next, AUT excitation signal reaches the TRM array, distanced to the metallic objects in half-wavelength of the excitation signal to reduce correlation between successive TRM probes. Finally, the signal reflects in the metallic walls and propagates following multipath propagation to the TRM. The Time Reversal algorithm is the solution of an electromagnetic wave inverse problem where divergent signals inside the TREC measured in the TRM are converted into a convergent signal refocused to the AUT. Time reversal algorithm requires measurements in the free-space time domain to neglect the effect of reflections from metallic objects.

*Key terms*—Impulse Response with 2D and 3D algorithm, free-space radiation pattern, azimuth, elevation, AUT, Time Reversal algorithm and reverberation environment.

# I. INTRODUCTION

Antenna is the main factor which affects total system communication performance in radar, mobile and satellite communications. Free-space radiation pattern is measured in an anechoic or semi-anechoic chamber where scatterings are suppressed by electromagnetic absorbing material in order to measure the antenna free-space radiation performance [1]. On the contrary, in the reverberating environment there are reflections, diffractions and scatterings which interfere with Antenna Under Test (AUT) signal free-space propagation [2]. Therefore, the measurements of antenna radiation pattern in a reverberation environment are faster to implement, cheaper and easier to modify than the measurements in an anechoic or semi-anechoic chamber.

Antenna radiation pattern estimation techniques calculate the free-space radiation pattern from measurements in a reverberating environment. In a reverberation environment the free-space signal is measured in the free-space time domain, this is the minimum time required between transmission and reception of the electromagnetic wave in antennas when they are facing each other. An antenna 3D radiation pattern estimation technique is proposed because it calculates the directivity with which an antenna transmits the excitation signal in every azimuth and elevation orientation angle.

Free-space radiation pattern is the standardized electromagnetic emission for electric and electronic equipment in ideal conditions, for the case of this work the equipment is antenna. Equipment Under

Test (EUT) free-space radiation pattern measurements have the purpose to determine equipment characteristics such as performance for applications in control and quality of products and investigation. However, the free-space or anechoic chamber is expensive because the cost is proportional to the quality of the absorbing material required in the construction of the chamber [1]. There are optional facilities to the reverberation environment where in reflections, diffractions and scatterings interfere with Equipment Under Test (EUT). These are Open Area Test Sites (OATS), Anechoic Chambers (AC) and Transverse Electromagnetic cells (TEM) [2]. In a reverberation chamber unintentional and intentional electromagnetic emission of electronic equipment are measured. Norm IEC 61000-4-21 establishes a common reference for using reverberation chambers to evaluate the performance of electronic equipment subjected to interference and determine equipment emission levels [3, 4].

Fast Fourier Transform (FFT) is a traditional technique which analyzes excitation signal transmission from AUT in a reverberating environment during the free-space time domain to estimate the AUT free-space radiation pattern. This is the time required by an electromagnetic wave to reach a reception probe. However, there is ambiguity in the free-space time boundaries [1]. Fast Fourier Transform algorithm (FFT) measures AUT signal in a reverberating environment, then it converts the signal from frequency to time domain where in replicas of the same signal are noticeable and can be gated or filtered in the free-space time domain. Next, FFT converts the AUT signal to the frequency domain as last step, this is the AUT

free-space radiation pattern [5]. Experiments in anechoic and semi-anechoic chamber using FFT antenna radiation pattern estimation techniques conclude that accuracy of FFT is dependent of frequency step $\Delta f$ and bandwidth $BW$ [5]. Test Zone Field (TZF) compensation technique reduces effect of extraneous electromagnetic fields created by reflections and scatterings to obtain an accurate AUT radiation pattern [6]. TZF states that using the deconvolution-based techniques limit extraneous fields compensation, increases the measurement time and the required equipment [6]. On the contrary, this work proves that deconvolution techniques are capable of accurately estimating the antenna radiation pattern with minimum equipment, time and provide accurate extraneous field model. Test Zone Field technique provides channel balance calibration and compensation of reflections and scatterings for multi-probe antenna [7]. Plane wave synthesis is a technique for near-field measurement of microwave antennas without anechoic environments that incorporates the principles of planar scanning system and plane wave synthesis to control the extent and the direction of the plane-wave flow at the antenna and the production of negligible low-field regions in the non-anechoic environment [8]. Matrix Pencil method (MP) is a high-resolution technique which calculates the coefficients of the $M$ exponentials expansion of the governing equation to estimate an antenna free-space radiation pattern [9]. MP technique accuracy depends on the number of exponentials $M$ and requires less bandwidth than FFT [5, 9]. The Oversampled Gabor transform (OGT) is a high-resolution technique which divides signals in frames to perform localized time-frequency and calculate the associated

coefficients to estimate the AUT free-space radiation pattern [10]. OGT technique achieves accuracy of less than 1 dB with respect to anechoic measurement in experiment with log-periodic antennas and avoids artifacts which may appear in MP method [10].

Impulse Response with 3D is an antenna 3D radiation pattern estimation algorithm for measurements in a reverberating environment and it is an extension from Impulse Response with 2D algorithm. The Impulse Response with 2D algorithm characterizes the reverberation environment with respect to every AUT azimuth angle orientation to obtain the impulse response in time and azimuth domain [1]. The Impulse Response with 2D requirements are several AUT measurements in azimuth domain and an advantage is that just a single frequency measurement is necessary to estimate the antenna free-space radiation pattern at that frequency. The Impulse Response with 2D algorithm limitation to estimate an accurate antenna free-space radiation pattern in a reverberation environment where in horizontal plane metallic objects are present is due to the poor characterization in the elevation domain as AUT measurement fixes the elevation and rotates only in azimuth angular orientation. Therefore, the Impulse Response with 3D algorithm proposes an antenna 3D radiation pattern estimation technique by using several measurements in azimuth and elevation domain at a single frequency. The elements of the antenna configuration system are Antenna Under Test (AUT) and probe antenna surrounded by metallic objects with finite conductivity $0 < \rho < \infty$. Impulse Response with 3D features deconvolution in azimuth and elevation angular domain.

The traditional applications of Time Reversal algorithm have been in ultrasonic fields using impulse diffraction theory to obtain the impulse response of the cavity in inhomogeneous medium [11]. In acoustics, the Device Under Test (DUT) produces waves which are transmitted inside a cavity where presence of echoes are strongly amplified. These echo signals are recorded in microphones. Afterwards, the Time Reversal algorithm employs the Time Reversal technique to reverse echo signals in time domain to reconstruct the initial acoustic wave. Source localization of acoustics waves based on Finite Difference Time Domain (FDTD) method using Time Reversal algorithm produces reversed signals in time domain focused to the location of the source [12]. Time Reversal algorithm applications in electromagnetics are generation of directive wave-fronts inside Time Reversal Electromagnetic Chamber (TREC) [13], Time Reversal Multiple Signal Classification (TR-MUSIC) imaging [14], single-antenna Time Reversal imaging based on Independent Component Analysis (ICA) [15], electromagnetic source synthesis by Reversed Transmission Line Matrix method (TLM) [16] and enforcing deterministic polarization in a reverberating environment where coherently polarized pulse fields are generated [17]. Synthetic Impulse Microwave Imaging System (SIMIS) is an array of Ultra Wide Band (UWB) antennas which image targets in a reverberation environment using the Time Reversal algorithm [18]. Time Reversal Mirror (TRM) provides imaging in the UWB using Through Wall Radar (TWR) technique [19]. Radar experiments using the Time Reversal algorithm in the microwave range report Decomposition of the Time Reversal Operator (DORT) for antenna free-space radiation pattern

estimation as the first experiment in the frequency range from 2 GHz to 4 GHz [20].

Time Reversal theory for electromagnetics has been developed since year 1999 and was oriented to acoustics or ultrasonic wave problems. Applications and experiments of Time Reversal theory [11-20] have led to the creation of the Time Reversal Electromagnetic Chamber (TREC). TREC elements are Antenna Under Test (AUT), Virtual Probe Array (VPA) and Time Reversal Mirror Antenna (TRM), all surrounded by four metallic objects with the form of walls [21]. Time Reversal algorithm is employed in a complex reverberating environment where electromagnetic reflections, diffractions and scatterings as specular or mirror-like reflection, edge or multiple diffraction, coupling and creeping waves interfere with AUT signal [22]. AUT transmits a signal which is sampled by VPA circular array of half-wavelength dipole antennas which are highly correlated because distance between VPA element is less than AUT wavelength when it operates in the frequencies from 2 to 3 GHz. Measurement of each dipole antenna can be omitted because Shannon sampling distance decimates VPA measurement, therefore, the harmonic filtering procedure features a spatial average which approximates VPA measurement to the antenna free-space radiation pattern [21]. Next, the AUT signal reaches Time Reversal Mirror linear array (TRM), a second array of half-wavelength dipole antennas uncorrelated between its elements because successive TRM dipoles are spaced in more than AUT excitation signal wavelength. Afterwards, reflections, diffractions and scatterings are produced in

TREC when AUT signal reaches metallic objects with the form of walls. Time Reversal principle is to reverse in time or conjugate in frequency the signal measured in TRM in free-space conditions, this happens before excitation signal reaches cavity walls, the time is $t_{free-space} = l/2c$ where l is the minimum distance between AUT and metallic objects, and c is speed of light. TRM retransmits conjugated signal in frequency or reversed signal in time to VPA circular array by means of the Channel Matrix function (CM) as medium of transmission. Next, original signal converges in the AUT as if AUT would have initially transmitted signal in time or frequency. Key factor to achieve convergence of different signal components and convert them in AUT signal in a reverberating environment is the calculation of an accurate Channel Matrix. Pyramidal Horn, Yagi Uda, Helical or other antenna can be employed as AUT to calculate the Channel Matrix because CM does not change as long as the rest of the TREC elements are not modified by exception of the AUT.

To estimate the antenna free-space radiation pattern in the reverberating environment the Impulse Response with 3D algorithm is proposed, a second technique, the Time Reversal algorithm is implemented from the references of this work. Modelling and simulation of Horn, Yagi Uda and Helical antennas in the software WIP-L, a Method of Moments (MoM) based electromagnetic solver for metallic and dielectric structures. The design of the reverberation environment will have implications in its frequency range of analysis and number of modes [3]. Chamber dimensions are inversely proportional to the excitation signal lowest frequency, (e.g. at 80

MHz it is required a chamber volume of 10,000 $\lambda^3$, where $\lambda = c/f$, $\lambda$ is wavelength, c is speed of light in free-space, f is excitation signal lowest frequency) [3]. Reverberating environments possess metallic objects with finite conductivity $0 < \rho < \infty$, where $\rho$ is conductivity in order to provide reliable and physically meaningful results not only in the reverberation chamber enclosure, but also in AUT and probe antennas should have finite conductivity because in a reverberating environment with Perfect Electric Conductors (PEC) (i.e. conductivity tends to infinite $\rho \to \infty$) the quality factor bandwidth is zero which would result in inaccurate antenna radiation pattern estimations [3]. Reverberating environments can be entirely closed surface (3D cavity), metallic objects in different planes with common junctions (2D cavity) or metallic objects in the same plane (1D). Next step is the processing of simulation data with MATLAB where antenna free-space radiation pattern algorithms have been implemented.

The objective for this work is to propose an antenna 3D radiation pattern estimation algorithm with higher accuracy than the Impulse Response with 2D algorithm in reverberating conditions. The antenna 3D radiation pattern estimation algorithm should be capable of characterizing vertical, horizontal and oblique metallic objects accurately. Finally, establish a qualitative and quantitative comparison between Impulse Response with 2D and the proposed antenna 3D radiation pattern estimation technique. The objective for Time Reversal technique is to prove that Time Reversal algorithm is capable to estimate the antenna free-space radiation pattern. Next,

describe the factors which affect an accurate calculation of the free-space radiation pattern estimation with Time Reversal algorithm. Finally, state the benefits and applications of free-space radiation pattern estimation with Time Reversal technique.

In Chapter II, Theory and Exam, explanation of Impulse Response with 3D and Time Reversal algorithms, and description of its antenna configuration system components. In Chapter III, Numerical Method, modelling and simulation of numerical examples in WIP-L 3D electromagnetic solver, then, processing of simulation data with MATLAB where in the Impulse Response with 3D and Time Reversal algorithms are tested. Next, in Chapter IV, Results, analysis of results from Impulse Response with 3D and Time Reversal techniques through contour graphs of the antenna radiation patter power, antenna radiation magnitude and phase pattern, error of estimation graphs and quantifiers to measure the performance of the techniques. Finally, in Chapter V, Conclusions, announce of results and contribution of the thesis.

## II. THEORY AND EXAM

Antenna radiation pattern is the directivity with which an antenna transmits an electromagnetic wave to the environment. The antenna radiation pattern formula is

$$\mathrm{G_D}(\theta,\varphi) = \frac{4\pi W(\theta,\varphi)}{P_t}, \tag{1}$$

where $\theta$ and $\varphi$ stand for azimuth and elevation, respectively, $W(\theta,\varphi)$ is the maximum radiated power per solid angle $(\theta,\varphi)$ and $P_t$ is the total radiated power [23].

Antenna far-field mathematical model can be described with [24]

$$\mathrm{E}(\theta,\varphi) = \lim_{L\to\infty} \sum_{L=0}^{L} \sum_{m=-l}^{l} a_{lm} Y_l^m(\theta,\varphi), \tag{2}$$

where $\theta$ and $\varphi$ stand for azimuth and elevation, respectively, $Y_l^m(\theta,\varphi)$ is the scalar spheric harmonics function with level l and mode m, $a_{lm}$ are the electric field coefficients and $\mathrm{E}(\theta,\varphi)$ is electric field function. Scattering parameter interrelate incident and reflected waves of energy at input and output ports of a linear two-port network. Scattering parameters or S-parameters are obtained by the mathematical model of a two-port network. Linear two-port networks in Fig. 1 represents any electrical and electronic equipment, an antenna for the purpose of this work.

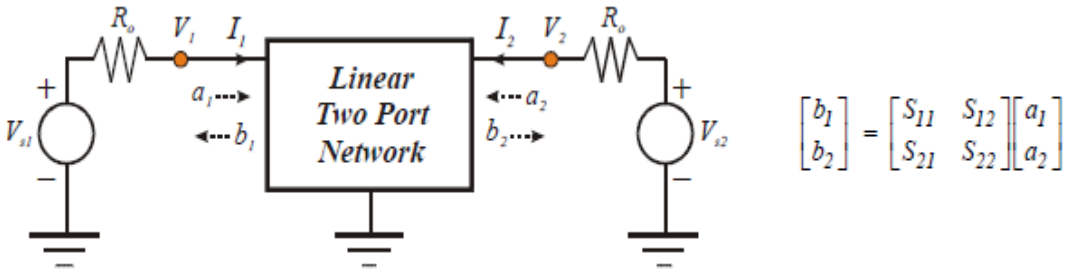


Fig. 1. Two port network representation and mathematical model.

The scattering parameters represent the antenna radiation pattern because the correlation of measured scattering or S-parameters equals the correlation of radiation pattern [25, 26], thus we have

$$\mathrm{R}(\theta,\varphi) = R_s(\theta,\varphi), \tag{3}$$

where $(\theta,\varphi)$ are azimuth and elevation angular domains, R is correlation of radiation pattern and $R_s$ is correlation of scattering parameters. The system auto-correlation is the convolution of the channel matrix function $\mathrm{h_{mn}}(t)$ with its time reversed version $\mathrm{h_{mn}}(-t)$. System auto-correlation in Time Reversal algorithm is [27]

$$\mathrm{R_{m,n}}(t) = \sum_{n=1}^{N} \hbar_{m,n}(-t) \otimes \hbar_{m,n}(t), \tag{4}$$

where $\otimes$ denotes convolution, $\hbar_{m,n}(t)$ is channel matrix, m is the index corresponding to the number of VPA probes, n is the index corresponding to the number of TRM probes and $\mathrm{R_{m,n}}(t)$ is the auto-correlation. From Eq. 3 and Eq. 4 is stated that $\hbar_{m,n}(t)$ function can be a measurement from the scattering parameters or radiation patterns where both will result in the auto-correlation function $\mathrm{R_{m,n}}(t)$.

### A. Impulse Response with 3D

It is a free-space radiation pattern reconstruction technique in magnitude and phase from a radiation pattern measured in a reverberating environment at a single frequency and varying the

orientation of the AUT in the azimuth and elevation planes. The AUT rotates in azimuth $\theta$ and elevation $\varphi$ angular domains to the orientation $(\theta_0, \varphi_0)$. The rotation point is AUT excitation point where electrons flow from metallic wire to its tip and convert in electromagnetic waves. AUT geometry and frequency of the excitation signal determine directivity gain, electric field and electric aperture characteristics of the antenna. Depending on previous characteristics an antenna may have two types of radiation pattern. The first type is the AUT with pencil-beam radiation pattern, a highly directive antenna with applications on radar. The second AUT type does not possess sharp-pencil radiation pattern and is disadvantageous on radar applications. The reverberation environment response when AUT does not possess pencil beam radiation pattern at frequency $f_0$ is

$$\widehat{\mathrm{A}}(\theta,\varphi)|_{f=f_0} = \frac{P_{reverberation}(\theta,\varphi)|_{f=f_0}}{P_{free-space}(\theta,\varphi)|_{f=f_0}} \ , \tag{5}$$

where $P_{reverberation}(\theta,\varphi)|_{f=f_0}$ is AUT radiation pattern measurement in reverberating environment at frequency $f_0$ and $P_{free-space}(\theta,\varphi)|_{f=f_0}$ is AUT radiation pattern measurement in free-space conditions at frequency $f_0$. Impulse Response with 3D technique formulas make use of discrete convolution in azimuth $\theta$ and elevation $\varphi$ angular domains in

$$P[\theta,\varphi] \otimes A[\theta,\varphi] = \sum_{n1=-\infty}^{\infty} \sum_{n2=-\infty}^{\infty} P_{[n1,n2]}.A_{[\theta-n1,\varphi-n2]}, \tag{6}$$

where $P[\theta,\varphi]$ and $A[\theta,\varphi]$ are discrete functions, n1 and n2 represent

the indices of the measurements in the azimuth and elevation domain, respectively. When the AUT possesses pencil beam radiation pattern the reverberating environment measurement is

$$\mathrm{P}_{\mathrm{reverberation}}(\theta,\varphi)_{t=t_0} = \mathrm{A}(\theta,\varphi)_{t=t_0} \otimes P_{free-space}(\theta,\varphi)_{t=t_0}, \quad (7)$$

where $P_{free-space}(\theta,\varphi)|_{t=t_0}$ is the AUT free-space measurement at time $t_0$, $\mathrm{P}_{\mathrm{reververation}}(\theta,\varphi)_{t=t_0}$ is AUT measurement in the reverberation environment at time $t_0$ and $\mathrm{A}(\theta,\varphi)|_{t=t_0}$ is the environment response at time $t_0$ which can be extracted from deconvolution, these three functions are in time domain. The calculation of the environment response when AUT has pencil-beam radiation pattern requires the environment response when the AUT does not possess a pencil-beam radiation pattern Equation (5). Environment response when AUT has pencil-beam radiation pattern formula is

$$\mathrm{A}(\theta,\varphi)_{t=t0} \otimes P_{free-space}(\theta,\varphi)_{t=t0} = \mathrm{F}^{-1}\{\hat{A}(\theta,\varphi)_{f=f0}.\mathrm{P}_{\mathrm{free-space}}(\theta,\varphi)_{f=f0}\}, \quad (8)$$

where $\hat{A}(\theta,\varphi)_{f=f_0}$ is the reverberation environment response when AUT does not possess pencil- beam radiation pattern at frequency $f_0$, $\mathrm{A}(\theta,\varphi)_{t=t0}$ is the environment response when AUT possesses pencil beam radiation pattern in time $t_0$, $P_{free-space}(\theta,\varphi)_{t=t_0}$ and $\mathrm{P}_{\mathrm{free-space}}(\theta,\varphi)_{f=f_0}$ are AUT free-space measurements in time $t_0$ and frequency $f_0$, respectively. Using deconvolution in Equation (8) the

environment response when AUT possesses pencil-beam radiation pattern is

$$\mathrm{A}(\theta,\varphi)|_{\mathrm{f=f_0}} = F\left\{\frac{F^{-1}\left[\ \hat{A}(\theta,\varphi)|_{f=f_0}\ .P_{free-space}(\theta,\varphi)|_{f=f_0}\right]}{F^{-1}[P_{free-space}(\theta,\varphi)|_{f=f_0}]}\right\}, \tag{9}$$

where $\hat{A}(\theta,\varphi)_{f=f_0}$ is the reverberating environment response when AUT does not possess pencil-beam radiation pattern at frequency $f_0$ and $P_{free-space}(\theta,\varphi)|_{\mathrm{f=f_0}}$is AUT measurement in free-space conditions at frequency $f_0$. Using deconvolution in Equation (7) the AUT free-space 3D radiation pattern is expressed as

$$P_{free-space}(\theta,\varphi)|_{f=f0}\ = F\left\{\frac{F^{-1}\left[P_{reverberation}(\theta,\varphi)|_{f=f0}\right]}{F^{-1}\left[A(\theta,\varphi)|_{f=f0}\right]}\right\}, \tag{10}$$

where $P_{reverberation}(\theta,\varphi)|_{f=f0}$ is AUT measurement in reverberation environment at frequency $f_0$, $A(\theta,\varphi)|_{f=f0}$ is the environment response when AUT possesses pencil-beam radiation pattern at frequency $f_0$ and $P_{free-space}(\theta,\varphi)|_{f=f0}$ is the AUT free-space radiation pattern estimation at frequency $f_0$.

The procedure to estimate the antenna 3D free-space radiation estimation has the following steps:

1. Obtain AUT free-pace reference and reverberating reference measurements in the azimuth $\theta$ and elevation $\varphi$ angular domains. These are $P_{free-space}(\theta,\varphi)$ and $P_{reverberation}(\theta,\varphi)$, respectively.
2. Calculate environment response when AUT possesses pencil-beam radiation pattern using Equation (5) and Equation (9) or Equation (7).

3. Switching AUT to other type of antenna obtain reverberation environment measurement $P_{reverberation}(\theta,\varphi)$ in the azimuth $\theta$ and elevation $\varphi$ angular domains at frequency $f_0$.
4. Estimate AUT free-space 3D radiation pattern $P_{free-space}(\theta,\varphi)$ using Equation (10).

## B. Time Reversal

The Time Reversal technique is an antenna radiation pattern estimation algorithm featured In the Time Reversal Electromagnetic Chamber (TREC). The elements of Time Reversal antenna configuration system or TREC are Antenna Under Test (AUT), Virtual Probe Array (VPA) and Time Reversal Mirror antennas (TRM) surrounded by metallic objects. Scattering or S-parameters represent radiation pattern measurements in TREC chamber where testing of antennas is carried on. The Channel Matrix function characterizes the interaction between Time Reversal Mirror antennas (TRM) with the Virtual Probe Array antennas (VPA) in the TREC. The Channel Matrix transfer function is expressed as

$$H_{mn}(f) = \frac{\hbar_a.(1+\Gamma_L)(1-\Gamma_S)}{\left(1-\hbar_b.\Gamma_L\right)\left(1-\Gamma_{IN}\Gamma_S\right)Z_L}, \quad (11)$$

where $\hbar_a$ is the Channel Matrix forward transmission measured with scattering parameter, $\hbar_b$ is the Channel Matrix reverse reflection, $\Gamma_L$ is load reflection, $\Gamma_S$ is source reflection, $\Gamma_{IN}$ is input reflection and $H_{mn}(t)$ is the Channel Matrix transfer function. The time reversal

algorithm in electromagnetics is the solution of a wave inverse problem in complex reverberating environments where reflections, diffractions and scatterings are amplified due to the characteristics of the two-dimensional cavity. The time reversal algorithm formula to estimate the AUT free-space radiation pattern in time domain is [21]

$$\hat{S}_n(t) = \sum_{m=1}^{M} y_m(-t) \otimes \hbar_{mn}(t), \tag{12}$$

where $y_m(-t)$ is a time-reversed signal measured at TRM in time domain, $\hbar_{mn}(t)$ is the Channel Matrix in time domain, m is the index of the number of elements of TRM array from m = {1; ..; M}, n is the index of the number of elements of VPA and $\hat{S}_n(t)$ is the estimated AUT free-space radiation pattern measured in VPA in time domain. The time reversal algorithm formula to estimate the AUT free-space radiation pattern in frequency domain is [21]

$$\hat{S}_n(f) = \sum_{m=1}^{M} Y_m^*(f) . H_{mn}(f), \tag{13}$$

where $Y_m^*(f)$ is a AUT conjugated signal of $Y_m(f)$ measured at TRM in frequency domain, $H_{mn}(f)$ is the system Channel Matrix in frequency domain, m is the index of the number of elements of TRM array from m = {1; ..; M}, n is the index of the number of elements of VPA and $\hat{S}_n(f)$ is the AUT free-space radiation pattern estimation in VPA in frequency domain. AUT signal estimation in the VPA with higher accuracy calculates the coefficients for each transmission from TRM and is expressed as

$$S_n(f) = \sum_{m=1}^{M} Y_m(f).\alpha_m.H'_{mn}(f), \quad (14)$$

where m is the index of the number of elements of TRM array where m = {1; ..; M}, n is the index of the number of elements of VPA, $Y_m(f)$ is the free-space measurement in TRM, the role of vector $\alpha_m$ is that of weight for the Channel Matrix and is computed independently by means of free-space array design techniques, $H'_{mn}(f)$ is the Channel Matrix before processing and $S_n(f)$ is the AUT signal estimation in the VPA. Hyugen's principle estimates the AUT measurement in TRM as validation of the Channel Matrix calculation. Hyugen's principle is [21]

$$Y_m(f) = \sum_{n=1}^{N} S_n(f).H_{mn}(f), \quad (15)$$

where n is the index of the number of elements of VPA from n = {1; ..; N}, m is the index of the number of elements of TRM array, $S_n(f)$ is the AUT measurement in the VPA in frequency domain, $H_{mn}(f)$ is the Channel Matrix and $Y_m(f)$ is the AUT estimated signal in the TRM in frequency domain.

### C. Physics of the software

Impulse Response with 3D and Time Reversal algorithms can estimate antenna radiation pattern and have different features and constraints for their implementations. WIPL-D is an electromagnetic solver which provides fast and accurate simulation and analysis in the

frequency domain of metallic and dielectric/magnetic structures such as antenna, scatterings and passive microwave circuits. WIPL-D solves current distribution, radiation pattern, near field, admittance, impedance at predefined points from metallic and dielectric structures [28].

"Flexible current modeling is based on polynomial approximation in conjunction with the Galerkin method applied to surface integral equations, resulting in extreme accurate method" [28]. The Galerkin Mehod is solved by using the Method of Moments by an approximation of the finite sum. The Method of Moments (MoM) is briefly described as

$$f(r) \cong \sum_{i=1}^{N} a_i f_i(r), \tag{16}$$

where $N$ is the order of approximation, $a_i, i = 1,..,N$, are unknown coefficients to be determined, $f_i(r), i = 1,..,N$, are known basis functions and $f(r)$ is an unknown function approximated by a sum [28].

As stated in Theory and Exam, scattering network parameters are proportional to those of radiation pattern coefficients. WIP-L calculates scattering parameter using a characteristic impedance of 50 $\Omega$. To measure the scattering parameters the procedure is the following: when an N-port is analyzed in antenna operation mode, the analysis is performed N-times because there are N-ports or excitation sources. In each excitation source a 1 volt generator is connected to a single port, while the rest remain in short circuit. Next, WIP-L calculates the complex currents in the port as these represent

the admittance parameters Y. Finally, the scattering parameters S, and also impedance parameters Z can be calculated with the matrix equation and characteristic impedance of 50 $\Omega$. Scattering or S-parameters matrix is [28]

$$[S] = \left([Z] + [50\Omega]\right)^{-1}\left([Z] - [50\Omega]\right), \tag{17}$$

where [Z] is impedance matrix, $[50\Omega]$ is a diagonal matrix whose all diagonal elements are equal to the characteristic impedance of 50 $\Omega$ and $[S]$ is scattering matrix. WIP-L simulation data is processed in MATLAB, a mathematic matrix based software for engineers and scientists, where in the proposed algorithms Impulse Response with 3D and Time Reversal have been a-priori implemented. Functions from Signal Processing toolbox in MATLAB are used as part of the main program which estimates the free-space antenna radiation pattern through Impulse Response with 3D and Time Reversal algorithms.

## III. NUMERICAL METHOD

The antenna system configuration refers to the elements required to estimate the free-space radiation pattern and they are stationary as the elements do not change in time with AUT as only exception. Horn pyramidal, Yagi Uda and Helical antennas are modelled and simulated as AUT or probing antenna at the frequency of 9 GHz in Fig. 2, Fig. 3 and Fig. 4, respectively.

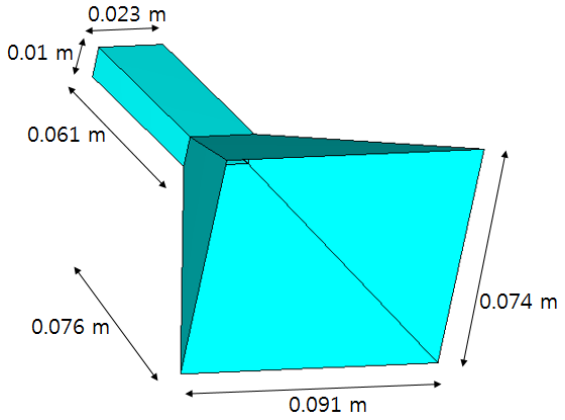


Fig. 2. Horn pyramidal antenna with center frequency at 9 GHz.

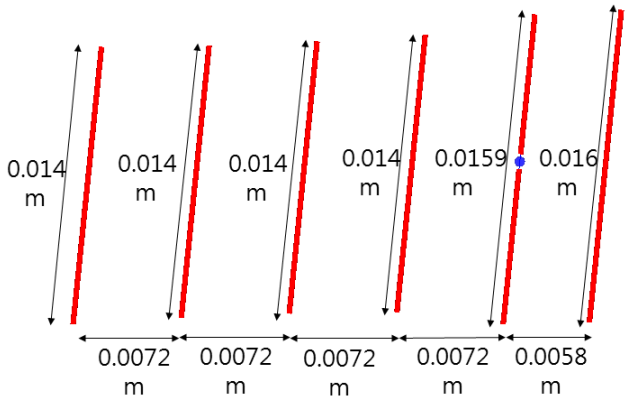


Fig. 3. Yagi Uda antenna with center frequency at 9 GHz.

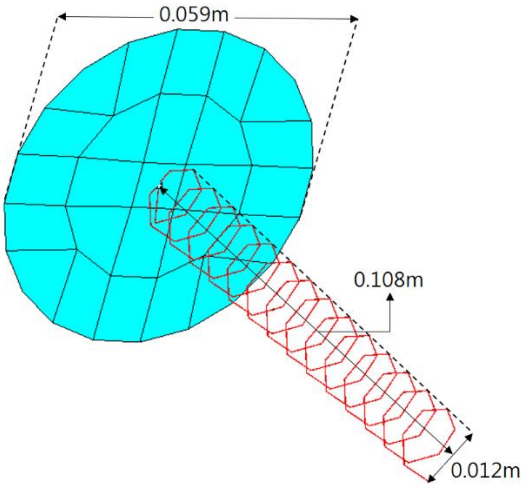


Fig. 4. Helical antenna with center frequency at 9 GHz.

### A. Antenna configuration system for Impulse Response with 3D

Antenna configuration system for Impulse Response with 3D has the following elements: AUT and probe antenna, both surrounded by metallic objects with finite conductivity $0 < \rho < \infty$.

AUT has wide radiation pattern in terms of power gain and bandwidth. The distance between the excitation ports of AUT and probe antenna is 2 m. AUT rotates in azimuth and elevation from -90° to 90° with the angle step of 5° to obtain an array of 37x37 data elements for each of the three AUT's: Pyramidal Horn, Yagi Uda and Helical antennas. Frequency analysis is performed at the fixed frequency of 9 GHz (SHF) which has applications in satellite TV, radiolinks and radar. The antenna system configuration for a free-space antenna radiation pattern measurement is presented in Fig. 5.

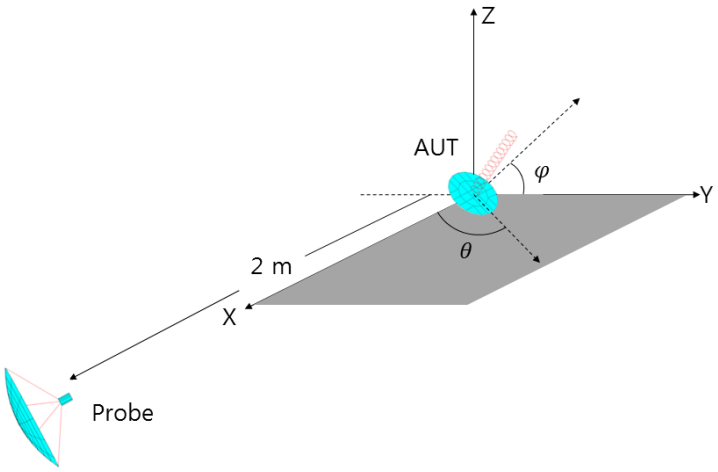


Fig 5. Antenna configuration system using Helical antenna as AUT and paraboloid antenna as probe in free-space conditions.

For the reverberation measurements there are two antenna system configurations with the only difference in the number of metallic objects. First reverberation measurement possesses one horizontal plane metallic object, a rectangle of 0.2 m x 0.5 m, equidistantly from AUT and probe with a height of 0.5m in Fig. 6. The probe is the Horn pyramidal antenna and AUT is switched between Horn pyramidal, Yagi Uda and Helical antenna. The AUT transmits electromagnetic waves which reflect, diffract and produce scatterings when they interact with the metallic objects of the reverberation environment. The response of Horn antenna as AUT is set as reference in order to estimate Yagi and Helical antennas free-space radiation pattern in Fig. 6. First reverberation measurement configuration system is described in Fig. 6.

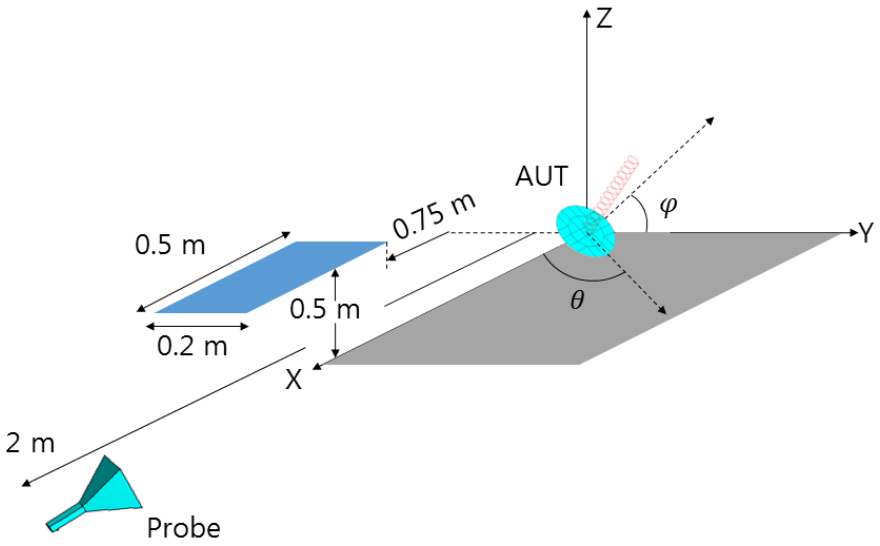


Fig. 6. Antenna configuration system using Helical as AUT and pyramidal Horn as probe surrounded by horizontal metallic object.

Second antenna system configuration possesses one vertical plane and one horizontal plane metallic objects, a rectangle of 0.5 m x 0.2 m and rectangle of 0.5 m x 0.187 m, respectively, equidistantly from the excitation ports of AUT and probe antenna with a distance of 0.5m from the XZ plane in Fig. 7. After that, the measurements follow the same fashion as in the first reverberation measurement antenna configuration system. The probe is the pyramidal Horn antenna and AUT is switched from pyramidal Horn, Yagi Uda and Helical antennas. The response of Horn antenna as AUT is set as reference in order to estimate Yagi antenna free-space radiation pattern in Fig. 7. Antenna configuration system for the second reverberation measurement is described in Fig. 7.

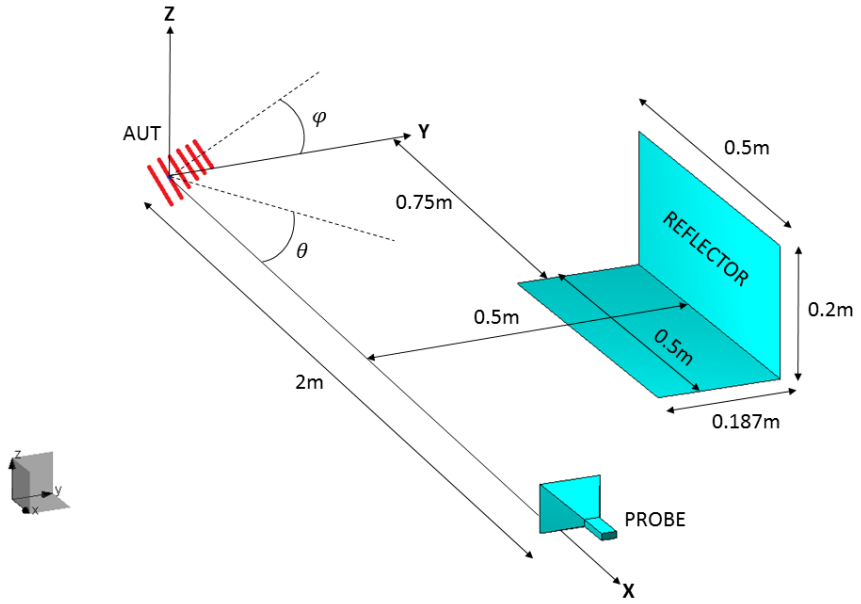


Fig. 7. Antenna configuration system using Yagi Uda as AUT Horn as probe surrounded by two metallic vertical and horizontal plates.

## B. Antenna configuration system for Time Reversal

It is featured in the Time Reversal Electromagnetic Chamber (TREC) which has the following elements: AUT, Time Reversal Mirror antennas (TRM) and Virtual Probe Array (VPA) surrounded by four metallic plates with finite conductivity $0 < \rho < \infty$ forming a metallic two-dimensional cavity of 8 m x 6.4 m which provides highly reflective properties to the cavity. AUT excitation port is in the center of the reverberating environment, VPA is a circular array of half-wavelength dipole antennas with radius of 2 m and distance of 0.2 m between successive dipoles which are highly correlated at 1 GHz and lower frequencies. Measurement of each dipole antenna can

be omitted because Shannon sampling distance decimates VPA measurement, therefore, the harmonic filtering procedure features a spatial average which approximates VPA measurement to the antenna free-space radiation pattern [21]. TRM is a linear array of half-wavelength dipole antennas located at 0.3 m of the 2-D metallic cavity and the distance between successive TRM dipoles is 1.0 m to provide uncorrelated measurement to each TRM dipole. Antenna system frequency response from 1 GHz to 3 GHz is analyzed (UHF) with a frequency step which varies from 10 MHz to 50 MHz. UHF is a frequency band with applications in TV broadcasting, GPS, mobile and satellite communications. Pyramidal Horn antenna is AUT in the Time Reversal configuration system and is the only element possible to modify. The antenna free-space radiation pattern measurement in Time Reversal technique simulation in Fig. 8.

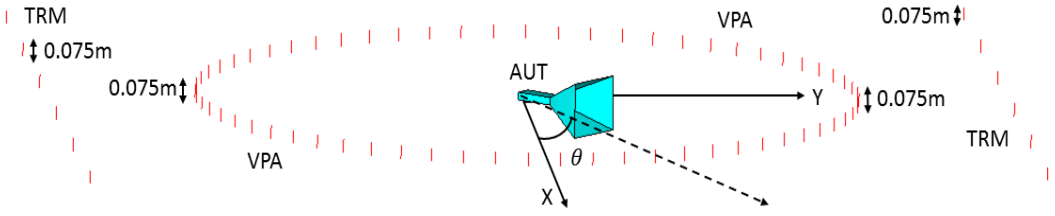


Fig. 8. Antenna configuration system using pyramidal Horn as AUT, 64 half-wavelength dipole antennas in a circular array (VPA) and 12 half-wavelength dipole antennas in linear array (TRM).

The Time Reversal Electromagnetic Chamber (TREC) is an environment where reflections, diffractions and scatterings interfere

with the AUT main signal. In the Time Reversal antenna configuration system or TREC the reverberation signals of AUT are recorded in VPA and TRM. The TREC radiation pattern measurement in Fig. 9.

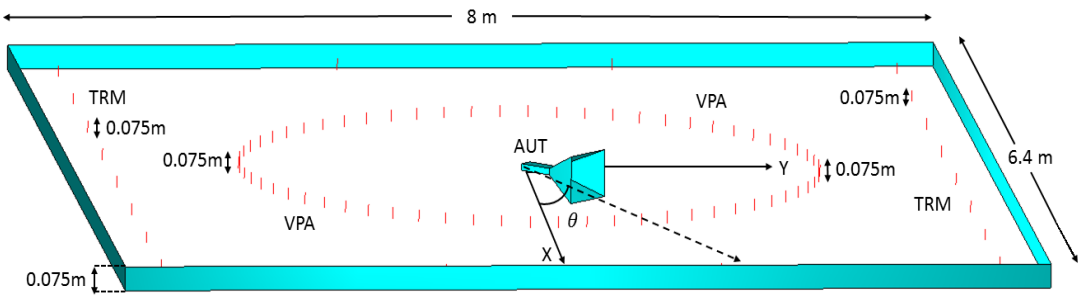


Fig. 9. Time Reversal Antenna configuration system or TREC using pyramidal Horn as AUT, 64 dipole antennas in a circular array (VPA) and 20 dipole antennas in linear arrays (TRM).

Modelling Time Reversal antenna configuration system (TREC) has to follow the next requirements: AUT with a wide radiation pattern in terms of power gain and bandwidth. VPA has highly correlated elements and as it has a circular form such that electromagnetic waves from AUT reach VPA at the same time permitting to sample the free-space AUT with minimum amount of interference in the near-range. On the other hand, the TRM located at short distance with the walls of the chamber, receives AUT radiated signals and reflection from the reverberation cavity is uncorrelated. Each TRM of the half-wavelength dipole antenna samples frequency

components of the initially transmitted signal, when they are uncorrelated each TRM provides additional information of the original signal. TRM and VPA antenna arrays are all composed of half-wavelength dipoles with length $\lambda/2$, where $\lambda$ is the wavelength obtained from the division of light-speed in free-space and central frequency of AUT excitation signal in order to achieve resonance in the antenna system. Considerations to analyze are the frequency range of analysis considering the number of modes are proportional to frequency and increase the interference, resolution or measurement test points, number of TRM's given that each TRM provides more information; however, they should be distanced a certain space to be uncorrelated to each other in a space limited by the reverberation environment.

### C. Quantifiers

Quantitative comparison of results uses averaged normalized error, maximum standard deviation and Euclidean distance metrics to provide indicators for the performance of the antenna free-space radiation pattern estimation using Impulse Response with 3D and Time Reversal techniques.

#### i. Averaged Normalized Error:

Computation of averaged normalized error for the Impulse Response results. The averaged in elevation domain normalized

error formula is

$$\mathrm{E}(\theta) = mean_{\varphi}\left[\frac{|\mathrm{S}(\theta,\varphi) - \hat{S}(\theta,\varphi)|}{\max\limits_{\varphi}|\mathrm{S}(\theta,\varphi)|}\right], \tag{18}$$

where $(\theta, \varphi)$ are the azimuth and elevation angular domains, respectively, $\mathrm{S}(\theta,\varphi)$ is the antenna free-space radiation pattern measurement and $\hat{S}(\theta,\varphi)$ is the antenna free-space radiation pattern estimation. Computation of averaged normalized error for the Time Reversal results. The averaged in VPA measurement normalized error formula is

$$\mathrm{E}(f) = mean_{VPA}\left[\frac{\left|S(f,VPA) - \hat{S}(f,VPA)\right|}{\max\limits_{VPA}|S(f,VPA)|}\right], \tag{19}$$

where $(f,VPA)$ represents the frequency $f$ and VPA dipole antennas, respectively, $\mathrm{S}(f,VPA)$ is the antenna free-space radiation pattern measured in frequency f and VPA dipole antennas and $\hat{S}(f,VPA)$ is the antenna free-space radiation pattern estimation in frequency f and VPA dipole antennas.

### ii. Maximum Standard Deviation:

$$\max(\sigma) = \max\left(\sqrt{E[(X-\mu)^2]}\right), \tag{20}$$

where $X$ is the difference of the free-space radiation pattern measurement S and the antenna free-space radiation pattern estimation $\hat{S}$, max is the maximum value of the vector and $\mu$ is the mean of $X$.

### iii. Euclidean Distance:

$$\|\mathrm{E}\| = \sqrt{\sum_{i=1}^{N} X_i^2}, \tag{21}$$

where $\mathrm{X_i}$ is the difference of the free-space radiation pattern measurement $\mathrm{S}$ and the antenna free-space radiation pattern estimation $\hat{S}_i$, and $\mathrm{N}$, $\mathrm{i} = 1; 2; 3; ..; \mathrm{N}$, is the number of elements of the matrix $\mathrm{X_i}$.

## IV. RESULTS

### A. Impulse Response with 3D

In Impulse Response with 3D algorithm, modelling and simulation has been carried in WIP-L at frequency of 9 GHz (SHF). Contour graphs have as axes the azimuth domain $\theta$ from -90° to 90° and elevation domain $\varphi$ from -90° to 90° , the level at every position ($\theta_0, \varphi_0$) is the radiation pattern power in decibels.

Contour graphs provide a qualitative comparison between Yagi antenna radiation pattern estimation with 2D, with 3D and free-space radiation pattern in Fig. 10 and Fig. 11. In Fig. 10 the antenna radiation pattern estimation from Fig. 6 using Impulse Response with 3D algorithm obtain shapes and power levels at azimuth and elevation that resemble more to the free-space space radiation pattern than the

Impulse Response with 2D algorithm.

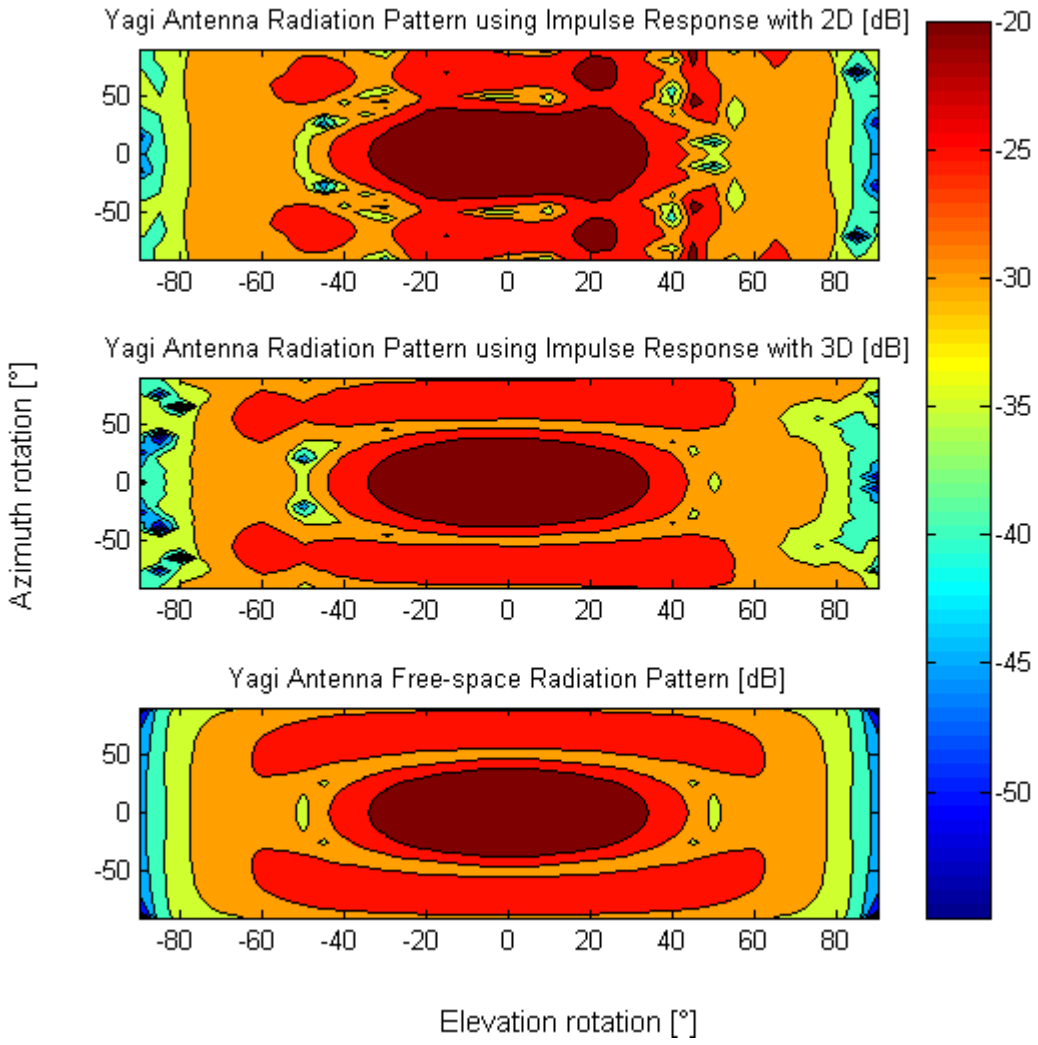


Fig. 10. Yagi Uda antenna contour graph comparison between Impulse Response estimation with 2D, with 3D and free-space radiation pattern at 9 GHz from Fig. 6.

In Fig. 11 the Yagi antenna free-space radiation pattern from Fig. 7 is estimated using Impulse Response with 3D. In the same fashion as

Fig. 10 the shape of the estimation for Impulse Response with 3D follows a similar pattern to that of the free-space measurement. Meanwhile, for Impulse Response with 2D the pattern has changed and areas have mixed with respect to the free-space measurement.

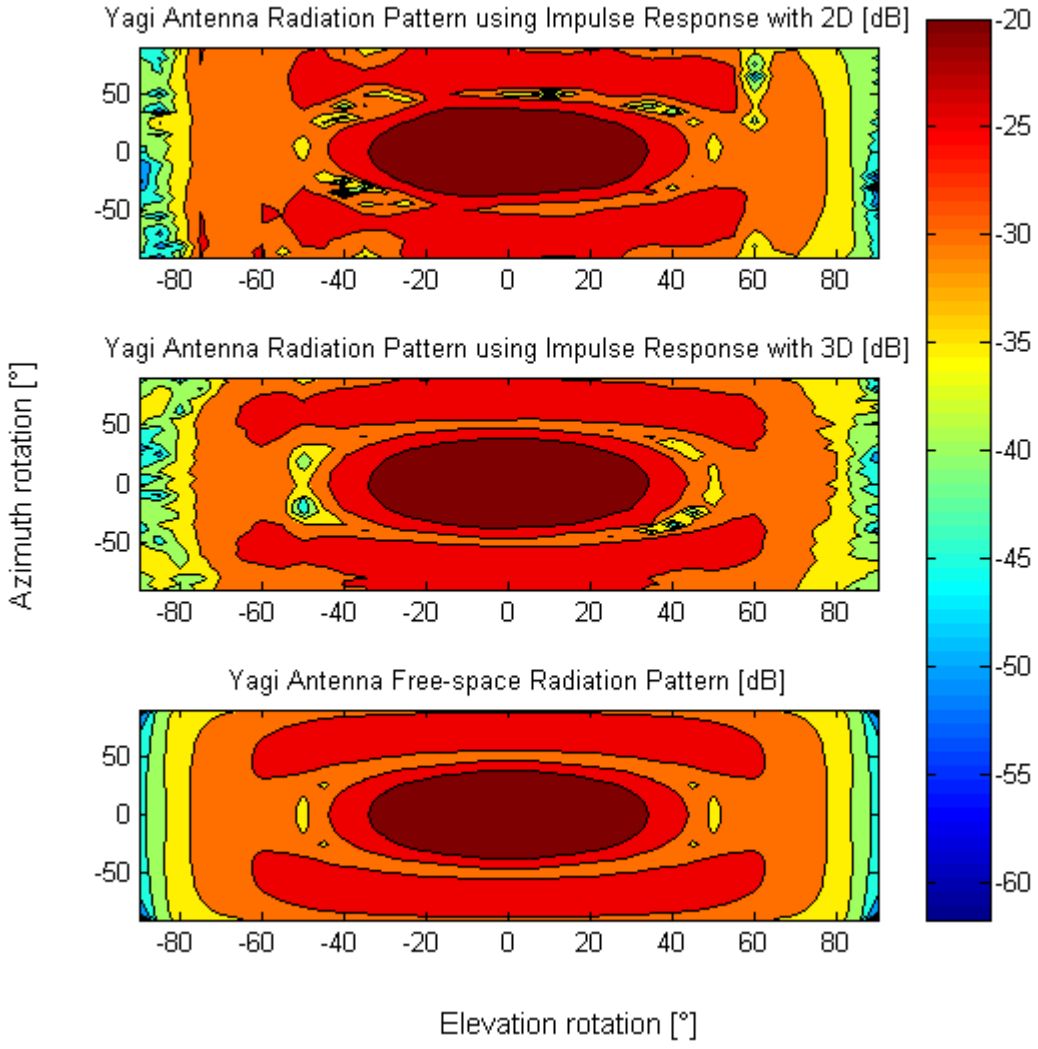


Fig. 11 Yagi Uda antenna contour graph comparison between Impulse Response estimation with 2D, with 3D, and free-space radiation pattern from Fig. 7.

Next, fixing the elevation in the contour graph results of antenna radiation pattern. The first type of graph is an amplitude pattern, which shows magnitude in decibels versus azimuth range from -90° to 90° at a fixed elevation. The second type is a phase pattern graph, which shows phase in radians versus azimuth range from -90° to 90° at a fixed elevation. All graphs are normalized with respect to the maximum value located at azimuth of 0° in the center of the azimuth axis.

Employing antenna configuration system from Fig. 6 with pyramidal Horn AUT as reference the Yagi and Helical free-space antenna radiation patterns in magnitude and phase are estimated using the Impulse response with 2D and 3D techniques, and fixing the elevation. Yagi antenna impulse response estimations with 2D and 3D, along with free-space and reverberation measurements fixing elevation at 15° , 20° and 25° are presented in the graphs of Fig. 12, Fig. 13 and Fig. 14. Helical antenna impulse response estimations with 2D and 3D, along with free-space and reverberation measurements fixing the elevation at 0° , 5° and 10° degrees are presented in the graphs of Fig. 15, Fig. 16 and Fig. 17.

Fig. 12(a) represents Yagi antenna estimation in magnitude of dB at 9 GHz and 15° of elevation. Impulse Response with 3D estimation resembles to free-space radiation pattern more than Impulse response with 2D estimation. Fig. 12(b) represents the comparison of the corresponding phases in radians.

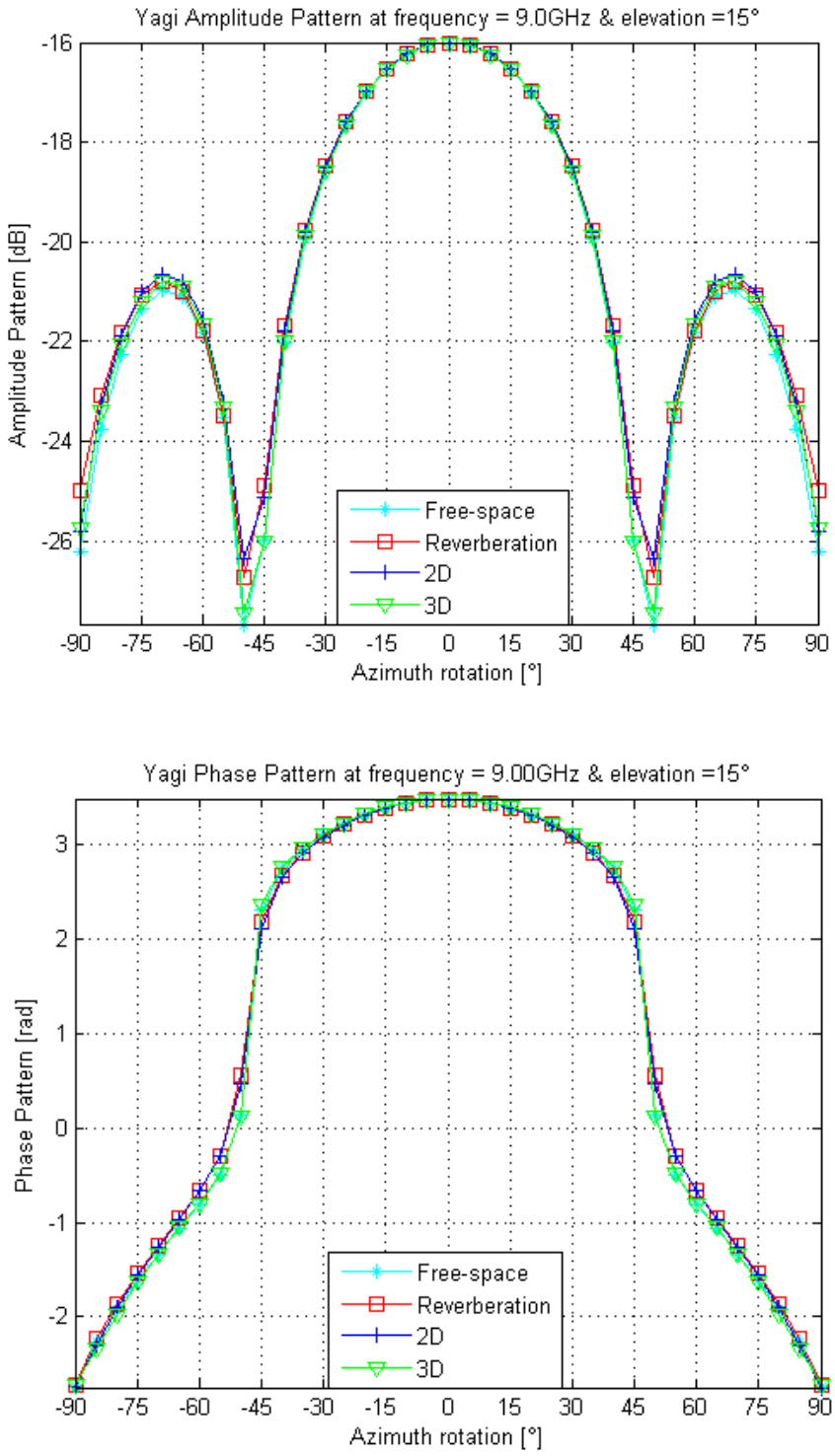


Fig. 12. (a) Amplitude pattern of Yagi antenna in dB at 9 GHz and 15° elevation. (b) Phase pattern rad at 9 GHz and 15° elevation.

Fig. 13(a) represents Yagi antenna magnitude of the reconstruction at 9 GHz and 20° elevation and Impulse Response with 3D estimation is closer to free-space measurement than Impulse Response with 2D estimation. Fig 13(b) provides the corresponding phase comparison. Fig. 14. (a) represents Yagi antenna magnitude of the reconstruction at 9 GHz and 25° elevation and in the main lobe the Impulse Response with 3D estimation follows the free-space radiation pattern measurement with higher accuracy than the Impulse Response with 2D. The Impulse Response with 2D shows poor performance as it remains closer to the reverberation measurement. Fig. 14(b) shows corresponding phase comparison. Fig. 15(a) represents Helical antenna magnitude of the reconstruction at 9 GHz and 0° elevation and in the main lobe the Impulse Response with 3D estimation follows the free-space radiation pattern measurement with higher accuracy than the Impulse Response with 2D estimation which shows poor performance as it remains closer to the reverberation measurement. Fig. 15(b) shows corresponding phase comparison. Fig. 16(a) represents Helical antenna estimation of magnitude at 9 GHz and 5° elevation and Impulse Response with 3D estimation is closer to free-space measurement than Impulse Response with 2D estimation. Fig. 16(b) provides corresponding phase comparison. Fig. 17(a) represents Helical antenna estimation of the magnitude at 9 GHz and 10° elevation. Impulse Response with 3D estimation follows the trajectory of the free-space measurement with higher accuracy than the Impulse Response with 2D estimation. Fig. 17(b) represents the comparison of the corresponding phases in radians.

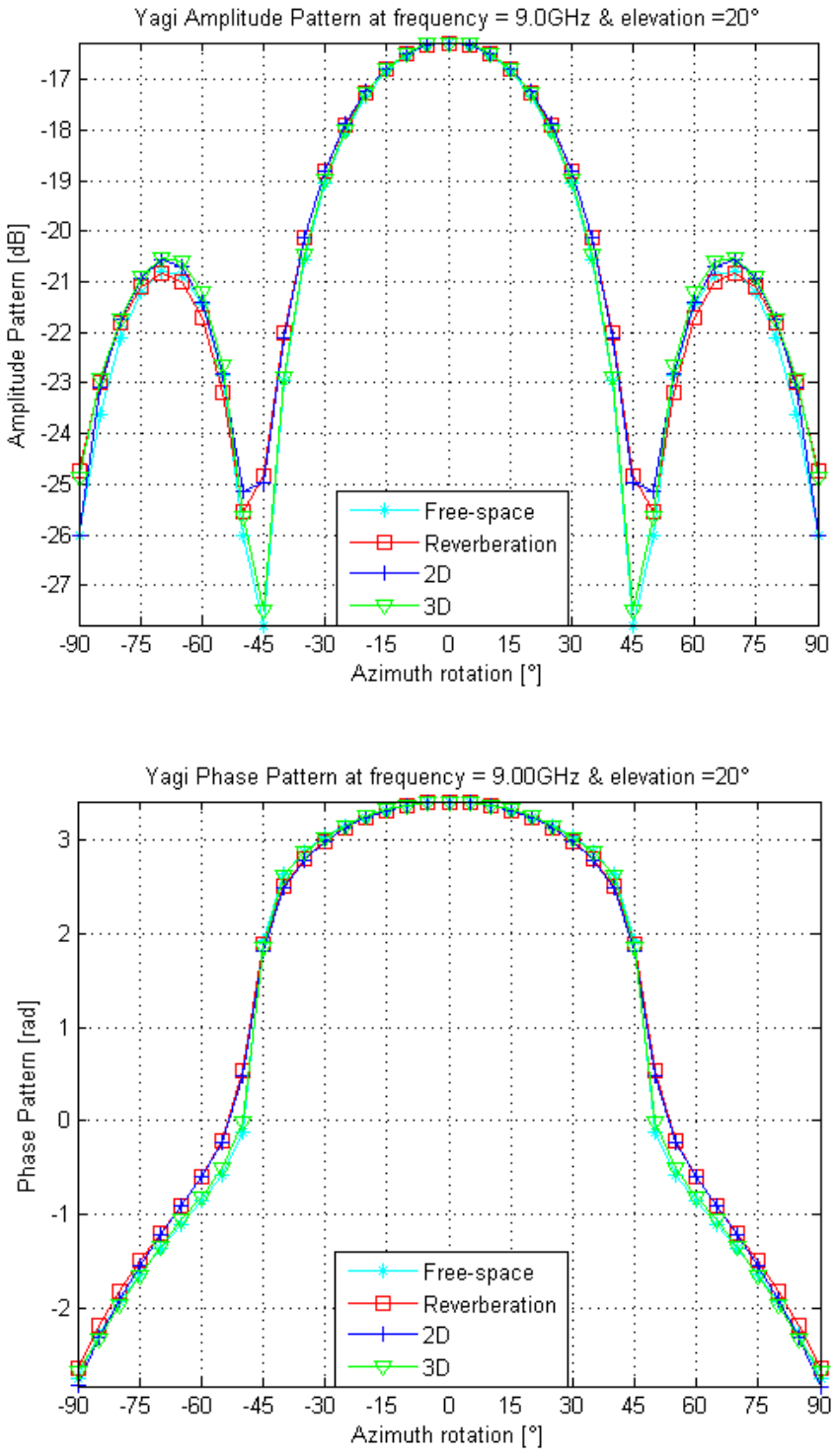


Fig. 13. (a) Amplitude Pattern of Yagi Antenna in dB at 9 GHz and 20° elevation. (b) Phase pattern rad at 9 GHz and 20° elevation.

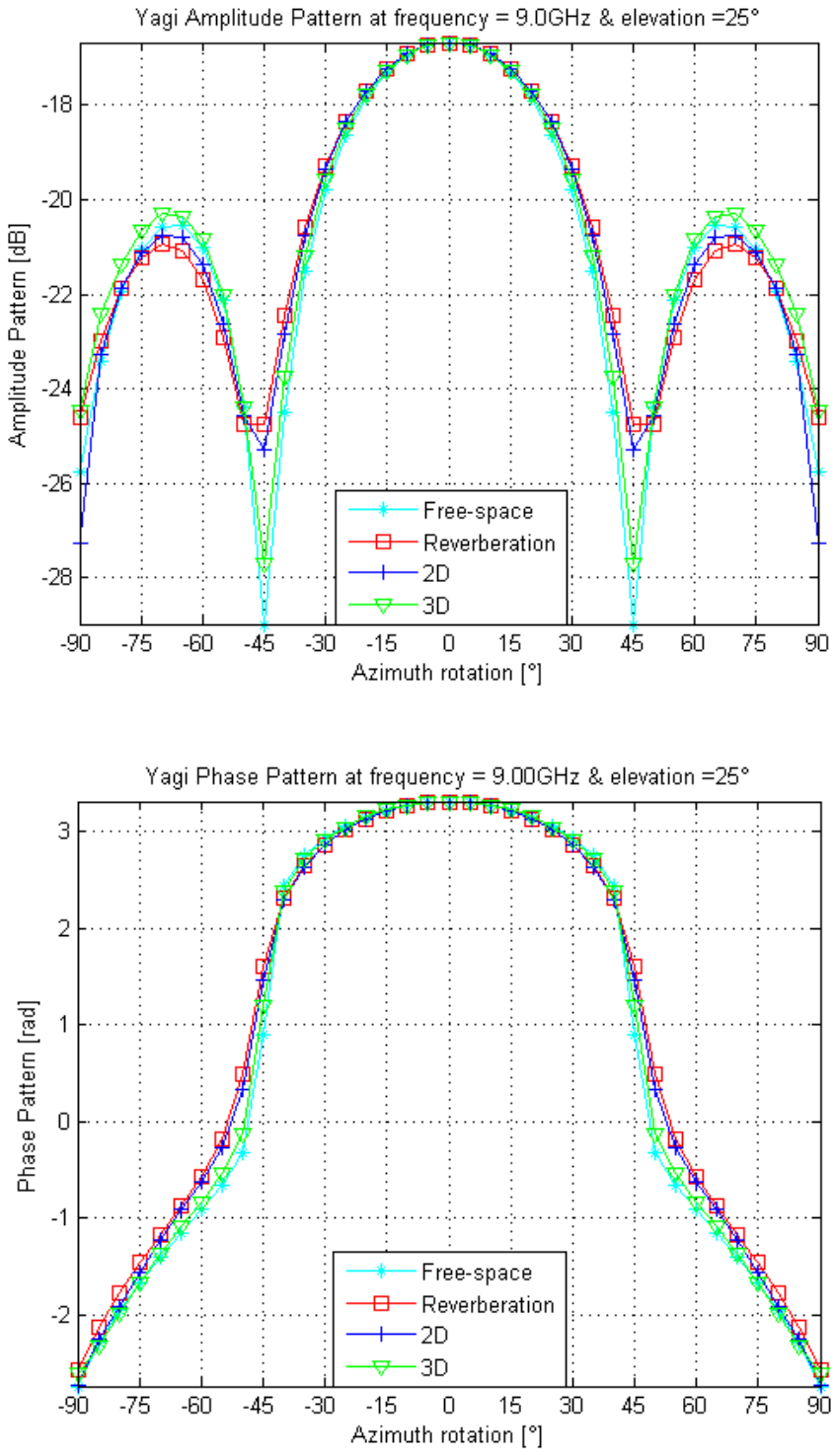


Fig. 14. (a) Amplitude pattern of Yagi Antenna in dB at 9 GHz and 25° elevation. (b) Phase pattern rad at 9 GHz and 25° elevation.

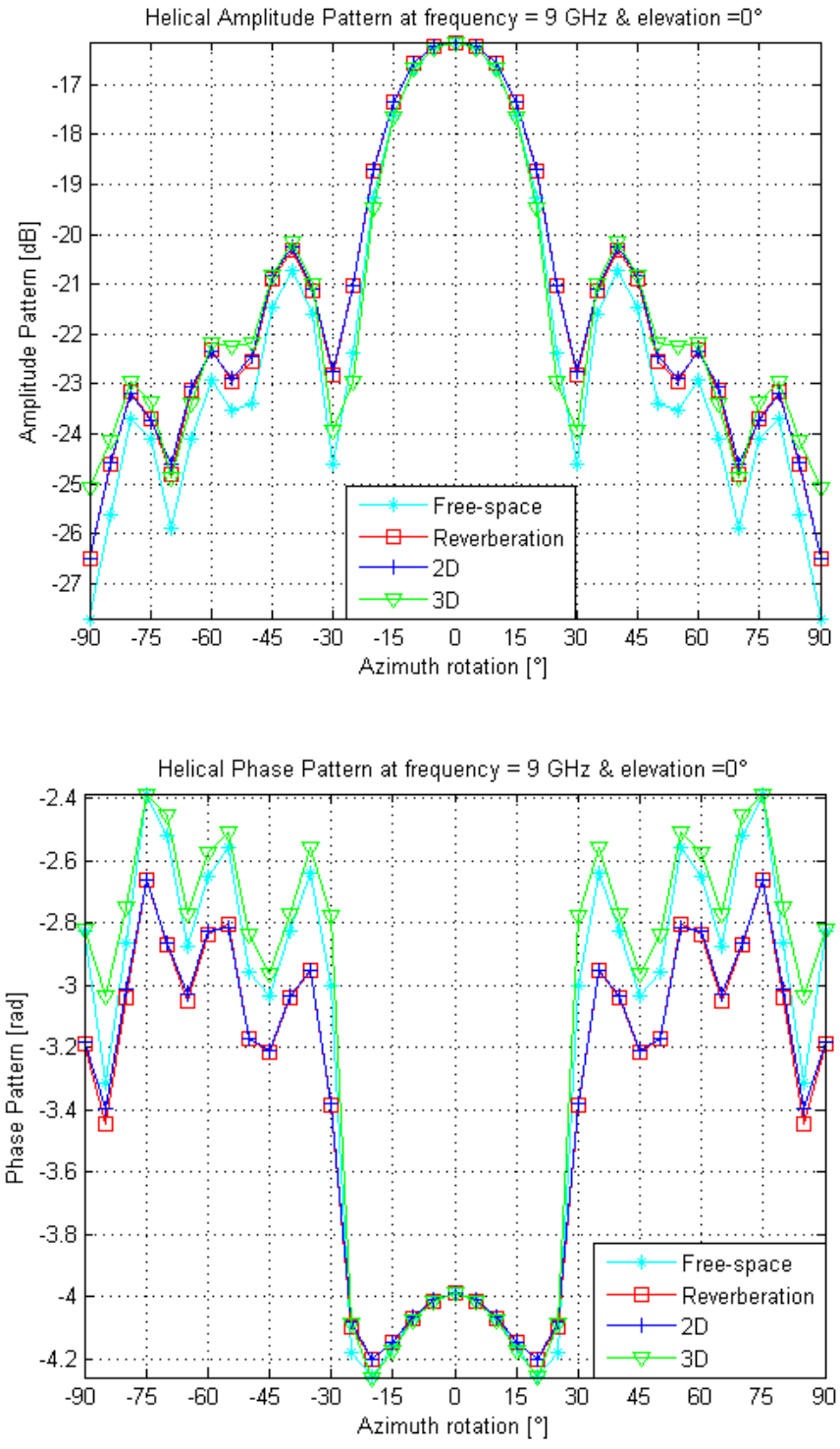


Fig. 15. (a) Amplitude pattern of Helical antenna in dB at 9 GHz and 0° elevation. (b) Phase pattern in rad at 9 GHz and 0° elevation.

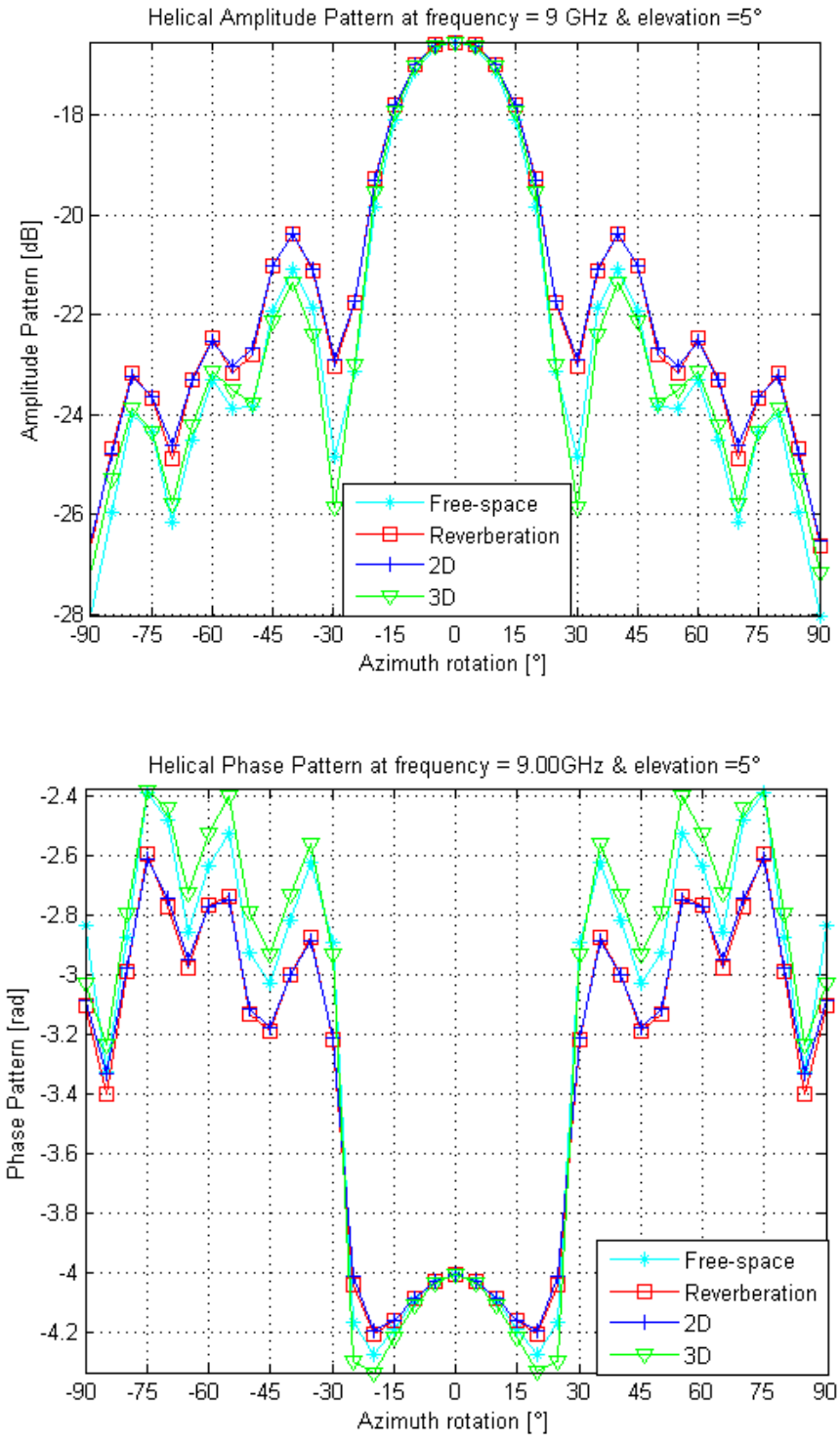


Fig. 16. (a) Amplitude Pattern of Helical antenna in dB at 9 GHz and 5° elevation. (b) Phase Pattern in rad at 9 GHz and 5° elevation.

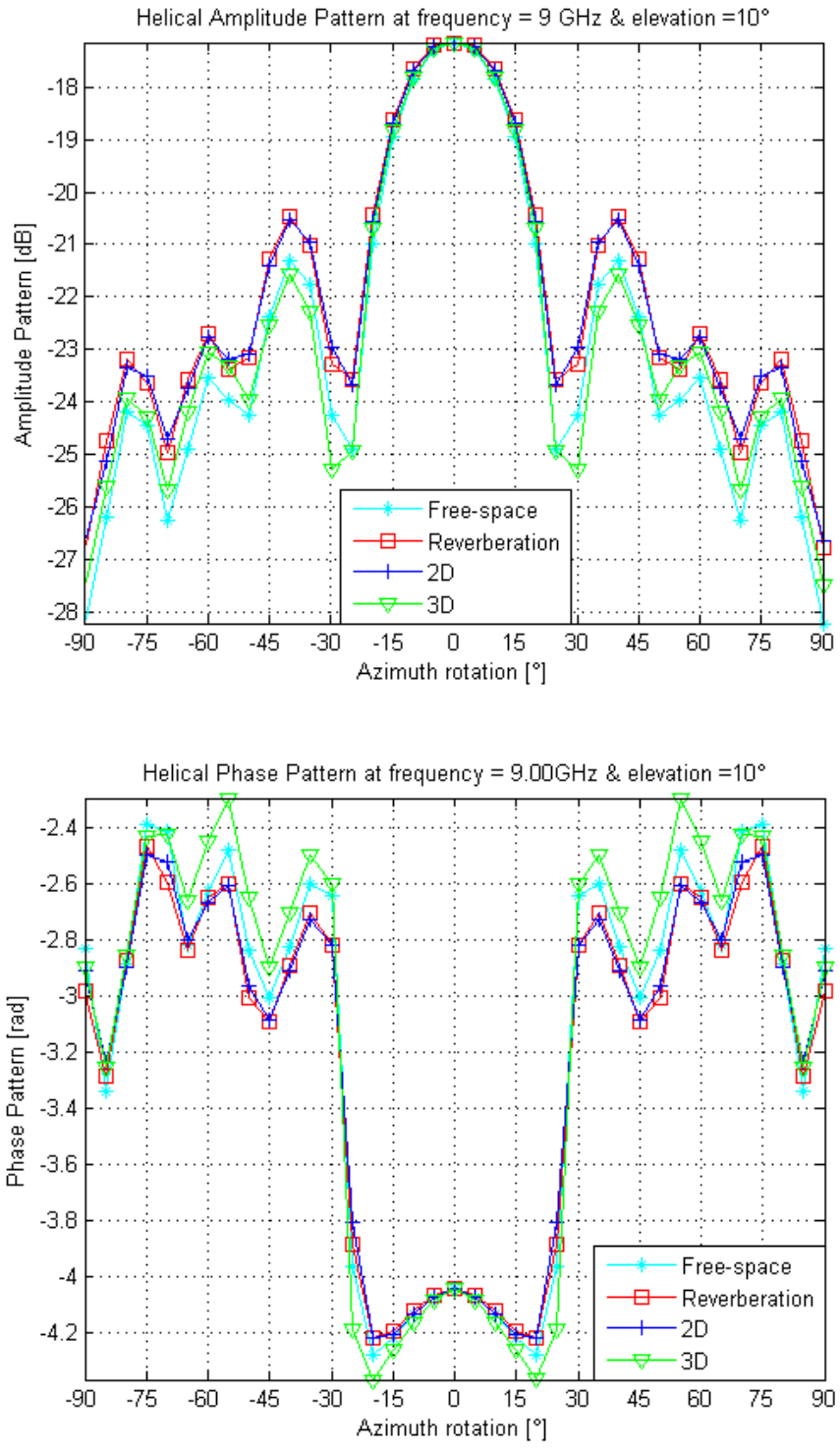


Fig. 17. (a) Amplitude Pattern of Helical antenna in dB at 9 GHz and 10° elevation. (b) Phase Pattern in rad at 9 GHz and 10° elevation.

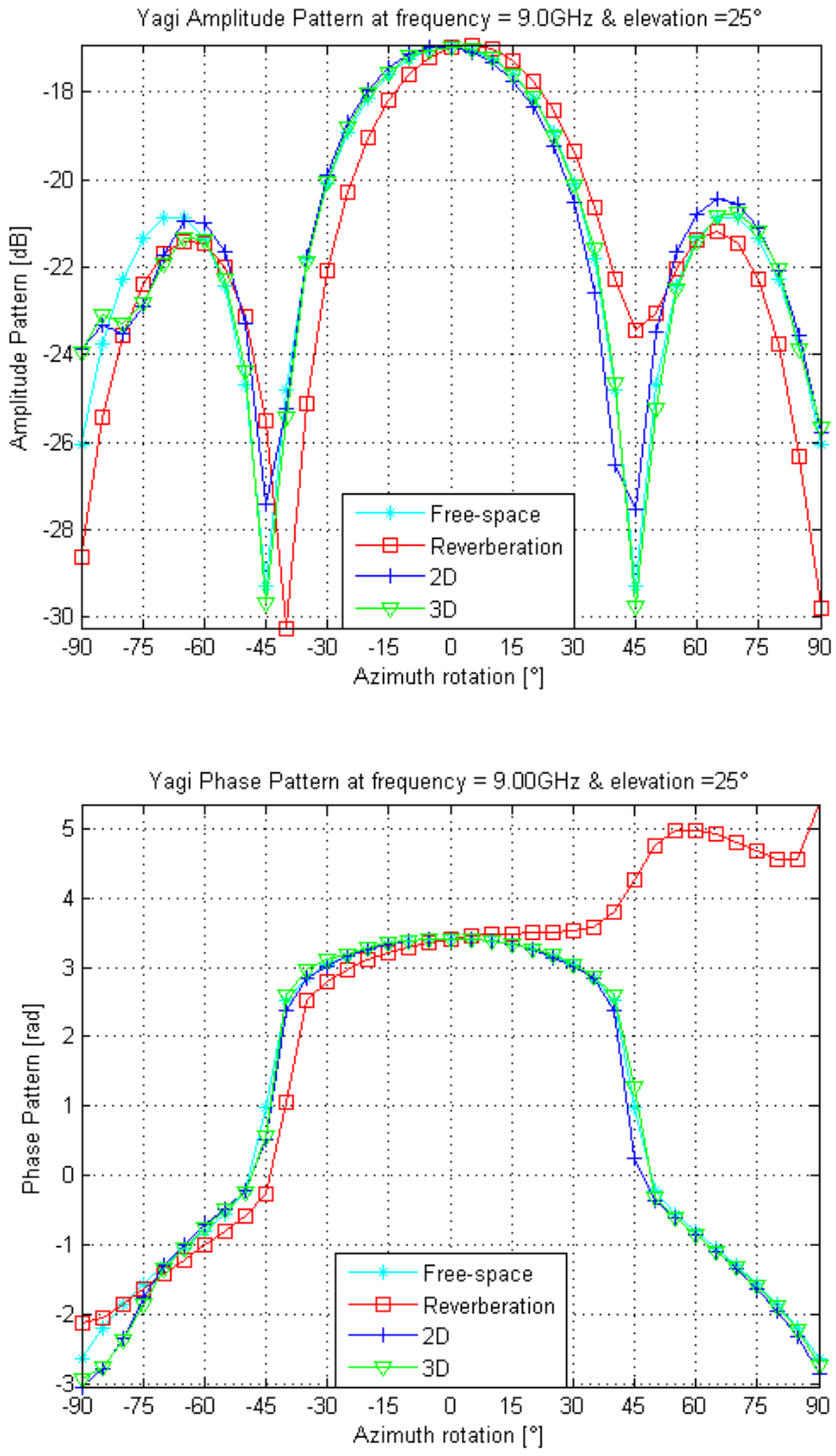


Fig. 18. (a) Amplitude pattern of Yagi antenna in dB at 9 GHz and 25° elevation. (b) Phase pattern in rad at 9 GHz and 25° elevation.

Employing antenna configuration system in Fig. 7 with Horn AUT as reference, the Yagi antenna free-space radiation pattern is estimated using the Impulse response with 2D and 3D algorithm, the Free-space and reverberation measurements are included in the graph. Yagi antenna magnitude and phase patterns fixing the elevation at 25° and 30° are presented in Fig. 18 and Fig. 19.

Fig. 18(a) represents the Yagi antenna estimation of the magnitude at 9 GHz and 25° elevation. Impulse Response with 3D estimation resembles to the free-space radiation pattern more than the Impulse Response with 2D estimation. Fig. 18(b) represents the comparison of the corresponding phase in radians.

Fig. 19(a) represents Yagi antenna estimation of the magnitude at 9 GHz and 30° elevation and Impulse Response with 3D estimation is closer to the free-space measurement than Impulse Response with 2D estimation. Fig. 19(b) provides corresponding phase comparison.

Afterwards, comparison is established using the average normalized error for antenna radiation pattern estimations with 2D and with 3D techniques in antenna configuration system in Fig. 6 and Fig. 7. Representation of Yagi and Helical antennas averaged in elevation normalized error in decibels versus azimuth range from -90° to 90° are shown in Fig. 20 and Fig. 21.

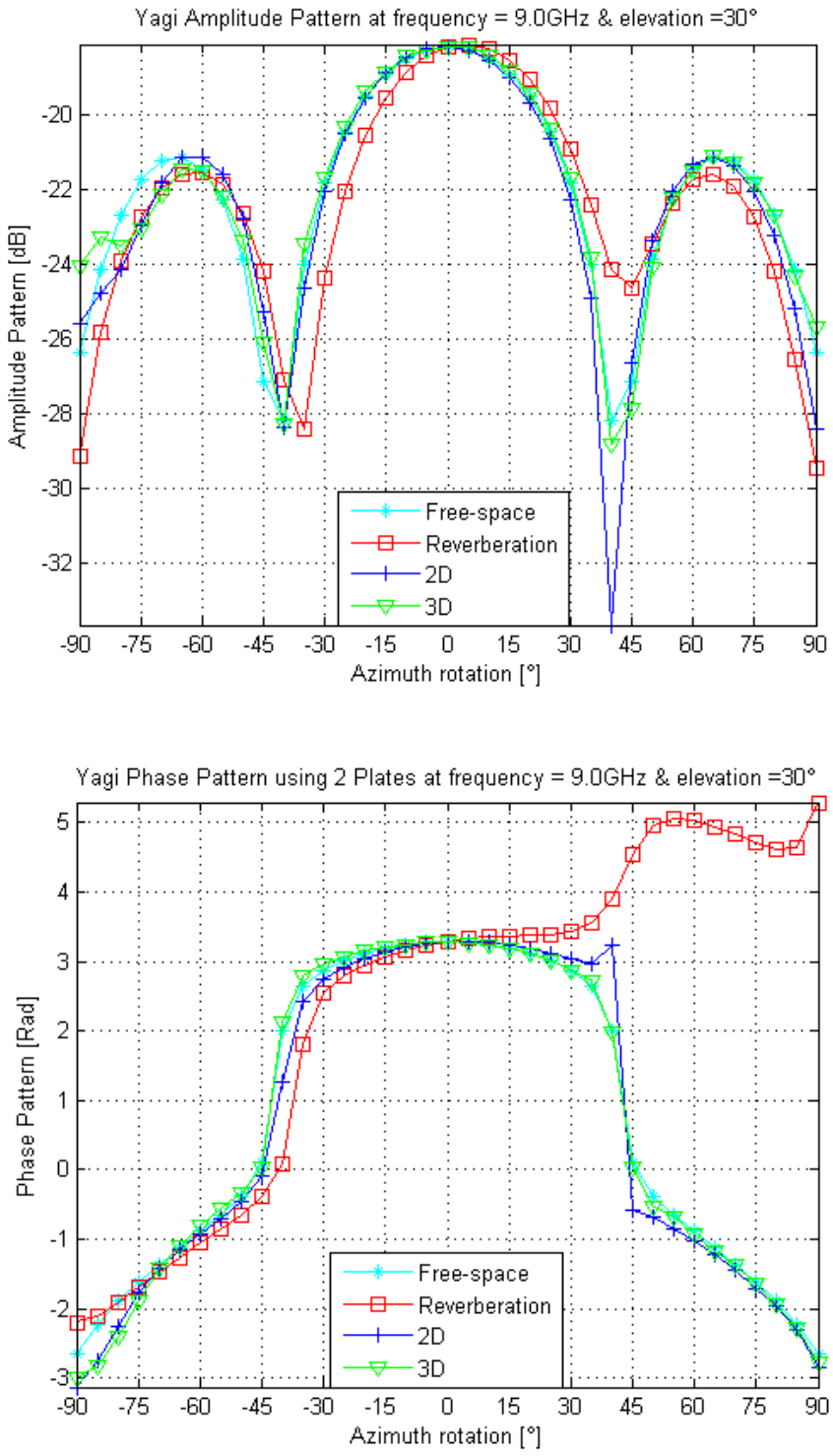


Fig. 19. (a) Amplitude pattern of Yagi antenna in dB at 9 GHz and 30° elevation. (b) Phase pattern in rad at 9 GHz and 30° elevation.

In Fig. 20 Yagi averaged in elevation normalized error in decibels versus azimuth from −90° to 90° represents the error in the estimation of Impulse Response with 2D, 3D and error of reverberation measurement with respect to the azimuth. Impulse Response with 3D normalized error is lower than the rest of errors in most if not all of the azimuth range orientations.

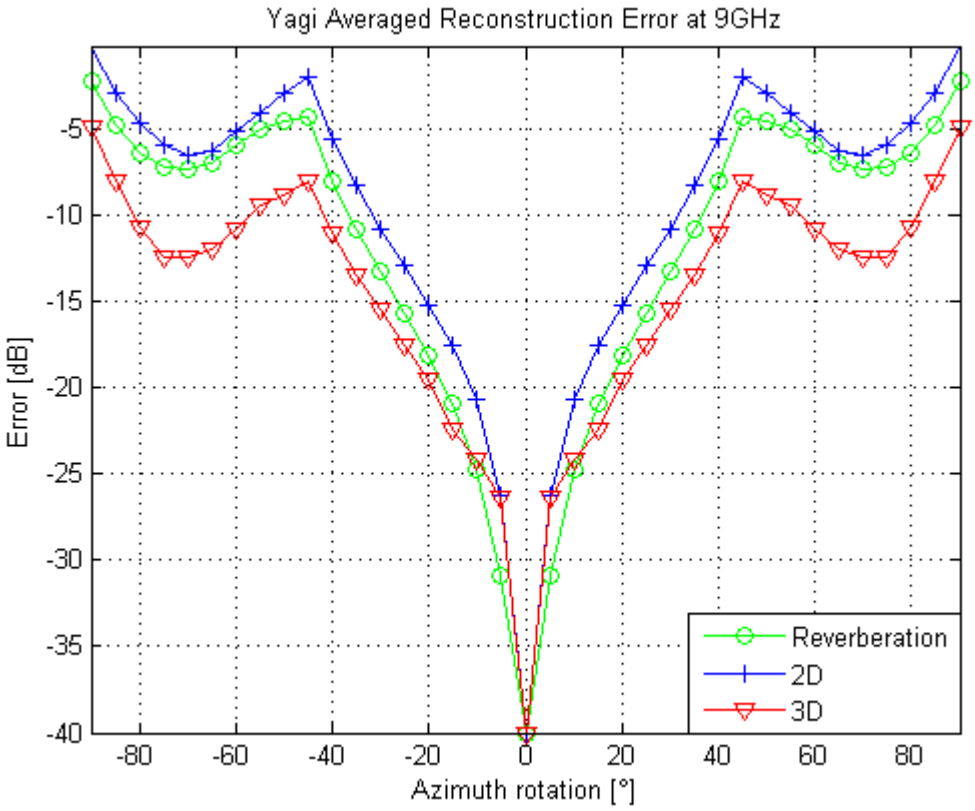


Fig. 20. Yagi antenna averaged normalized error of estimation at 9 GHz from Fig. 6.

In the same fashion, for Fig. 21, Helical antenna Impulse Response

with 3D normalized error is the lowest in all azimuth orientations.

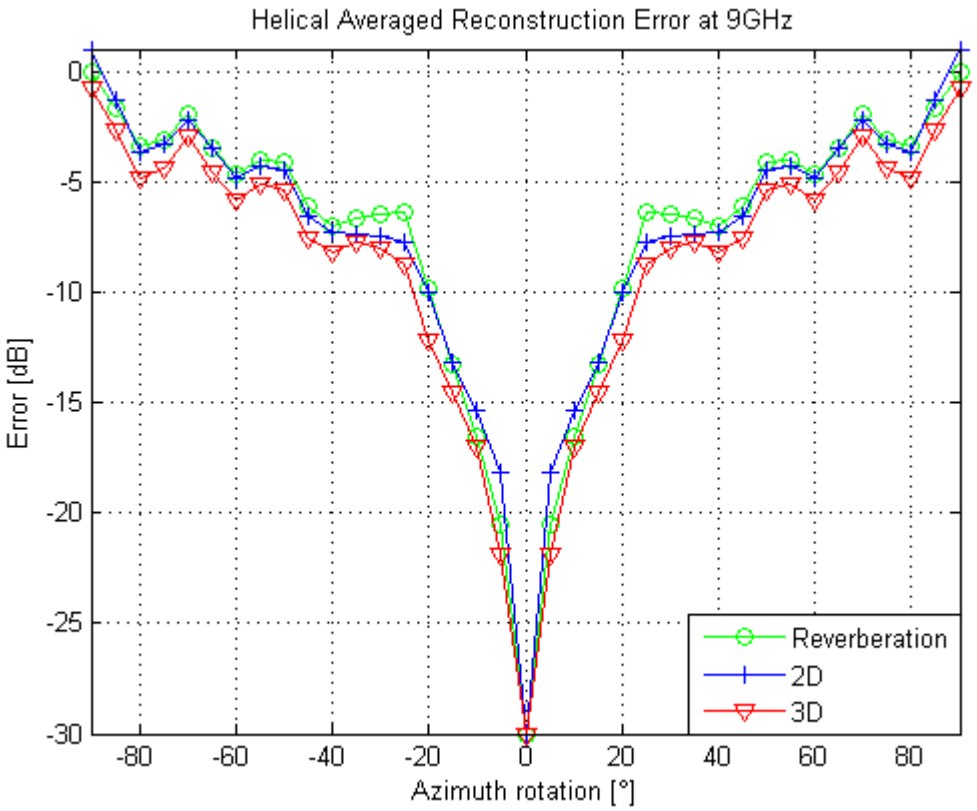


Fig. 21. Helical antenna averaged normalized error of estimation at 9 GHz from Fig. 6.

For the second reverberation environment in Fig. 7 where in vertical and horizontal metallic objects are present the comparison of the average normalized error for antenna radiation pattern estimation with 2D, with 3D and error of reverberation measurement in Yagi antenna is presented in Fig. 22. Fig. 22 the Impulse Response with 3D technique outperforms the Impulse Response with 2D technique

at all of the azimuth orientations.

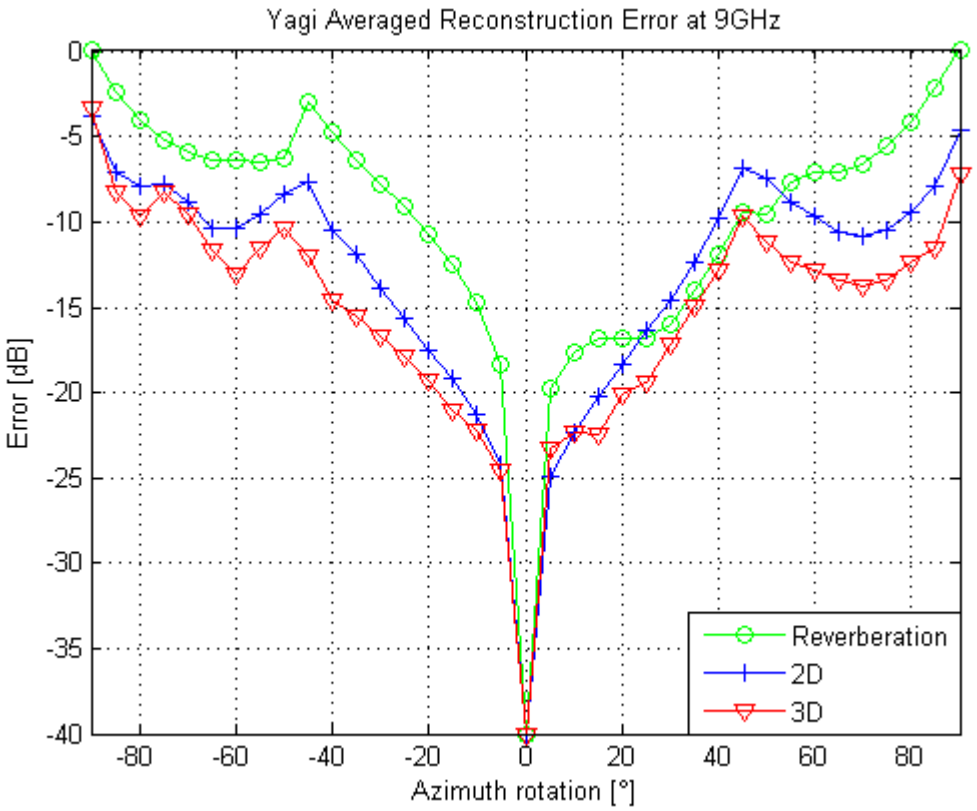


Fig. 22. Yagi antenna averaged normalized error of estimation at 9 GHz from Fig. 7.

Quantitative comparison of results uses average of the averaged normalized error, maximum standard deviation and Euclidean distance metrics to provide indicators of the antenna radiation pattern estimation performance of the Impulse Response with 2D and 3D in Table I and Table II.

In Table I. and Table II. there are summary of the results of antenna

configuration system in Fig. 6 using three metrics: the average of the averaged normalized error, maximum standard deviation and Euclidean distance. In Table I, Yagi antenna radiation pattern reconstruction with 3D performance is superior than reconstruction with 2D according to the three metrics. In Table II. Helical antenna radiation pattern reconstruction with 3D outperforms the reconstruction with 2D in the same fashion as Yagi antenna.

Table I. Yagi antenna radiation pattern error metrics in Fig. 6.

| Antenna | Measurement/ Error | Reverberation | Impulse Response with 2D | Impulse Response with 3D |
|---|---|---|---|---|
| Yagi | $E_{avg}(\%)$ | 18.79 | 27.66 | 7.97 |
| | $\sigma_{\max}$ | 0.0028 | 0.006 | 0.00085945 |
| | $Norm$ | 0.072 | 0.106 | 0.0227 |

Table II. Helical antenna radiation pattern error metrics in Fig. 6.

| Antenna | Measurement/ Error | Reverberation | Impulse Response with 2D | Impulse Response with 3D |
|---|---|---|---|---|
| Helical | $E_{avg}(\%)$ | 34.6 | 34.68 | 26.47 |
| | $\sigma_{\max}$ | 0.0025 | 0.0029 | 0.0014 |
| | $Norm$ | 0.0768 | 0.07 | 0.06 |

In table III, a summary of Yagi radiation pattern error in Fig. 7 shows performance of reconstruction with 3D is approximately 50% superior than reconstruction with 2D for three metrics and 3D $E_{avg}$ 6.53% is lower than 1dB.

Table III. Yagi antenna radiation pattern error metrics in Fig. 7.

| Antenna | Measurement/ Error | Reverberation | Impulse Response with 2D | Impulse Response with 3D |
|---|---|---|---|---|
| Yagi | $E_{avg}(\%)$ | 23.83 | 10.34 | 6.53 |
| | $\sigma_{\max}$ | 0.0032 | 0.0014 | 0.0008 |
| | $Norm$ | 0.0911 | 0.0361 | 0.0205 |

## B. Time Reversal

In Time Reversal algorithm modelling and simulation has been carried in WIP-L at the frequency range from 1 GHz to 3.0 GHz (SHF). Contour graphs axes are VPA measurement for 64 half-wavelength dipole antennas and frequency from 1 GHz to 3 GHz, the level at every position $(f, vpa)$ is the AUT radiation pattern power in decibels. Contour graphs provide a qualitative comparison between Horn antenna free-space radiation pattern estimation with Time Reversal algorithm, free-space and reverberation pattern measurement in Fig. 23 and 24. In Fig. 23 Pyramidal Horn antenna as AUT, VPA array of

64 half-wavelength dipoles antennas, TRM linear array of 20 half-wavelength dipoles, frequency range of analysis is from 1 GHz to 3.0 GHz and frequency step is 25 MHz. The Time Reversal algorithm estimates the AUT radiation pattern in the Virtual Probe Array (VPA) because VPA samples the AUT radiation pattern in each of its elements as a multi-probe antenna.

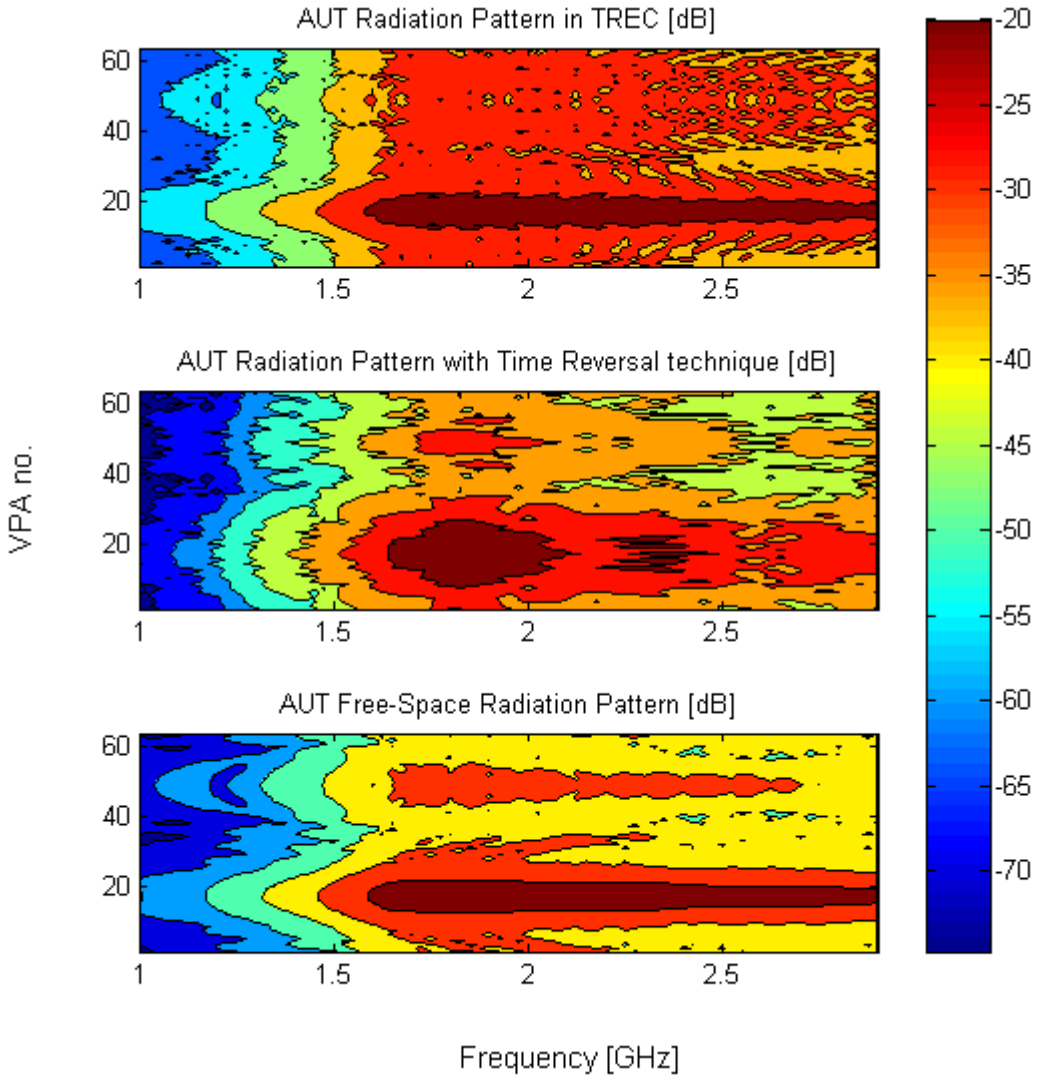


Fig. 23. Horn AUT radiation pattern comparison in dB with axes of VPA measurement and frequency range of [1; 2.9] GHz.

In Fig. 23 the AUT radiation pattern estimation with Time Reversal technique form resembles more to the free-space measurement than the reverberation environment measurement in form of the lobes and power levels. On the contrary, in the reverberation measurement the form is spread and power increases in VPA dipoles measurement from number 40 to 64.

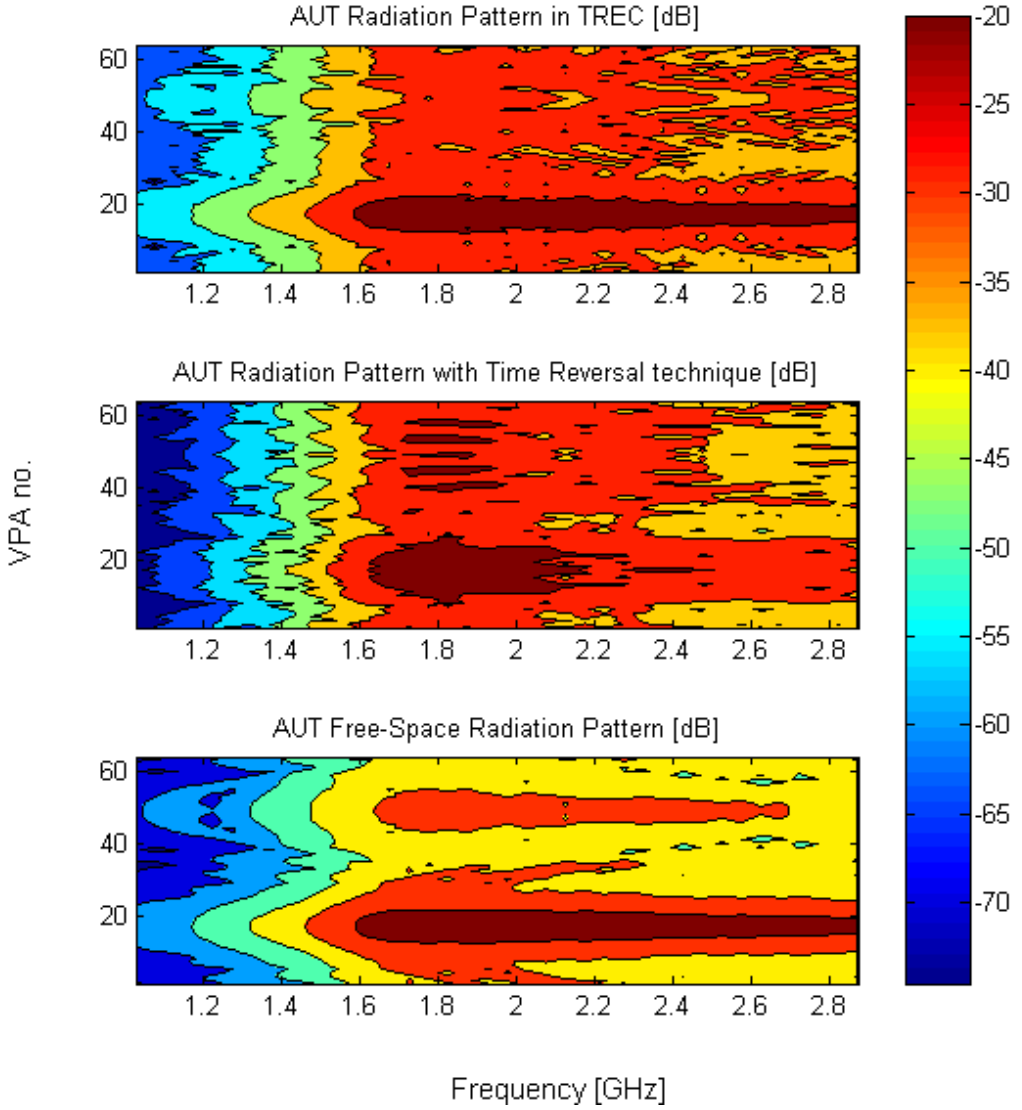


Fig. 24. Horn AUT radiation pattern in dB comparison with axes of VPA measurement and frequency range of [1; 2.9] GHz.

Next, in Fig. 24 modelling and simulation of Time Reversal with Horn as AUT, VPA of 64 half-wavelength dipoles, TRM of 20 half-wavelength dipoles and frequency range of analysis is from 1.25 GHz to 2.875 GHz with frequency step of 44 MHz.

Fig. 24 represent, in order, the AUT radiation pattern measurement in TREC, Time Reversal technique estimation and free-space measurement. Quality of the estimation with Time Reversal technique has a similar appearance in form and power with the reverberation environment measurement as resolution of the measurement has decreased due to the increase in the frequency step (from 25 MHz to 44 MHz) with respect to first simulation.

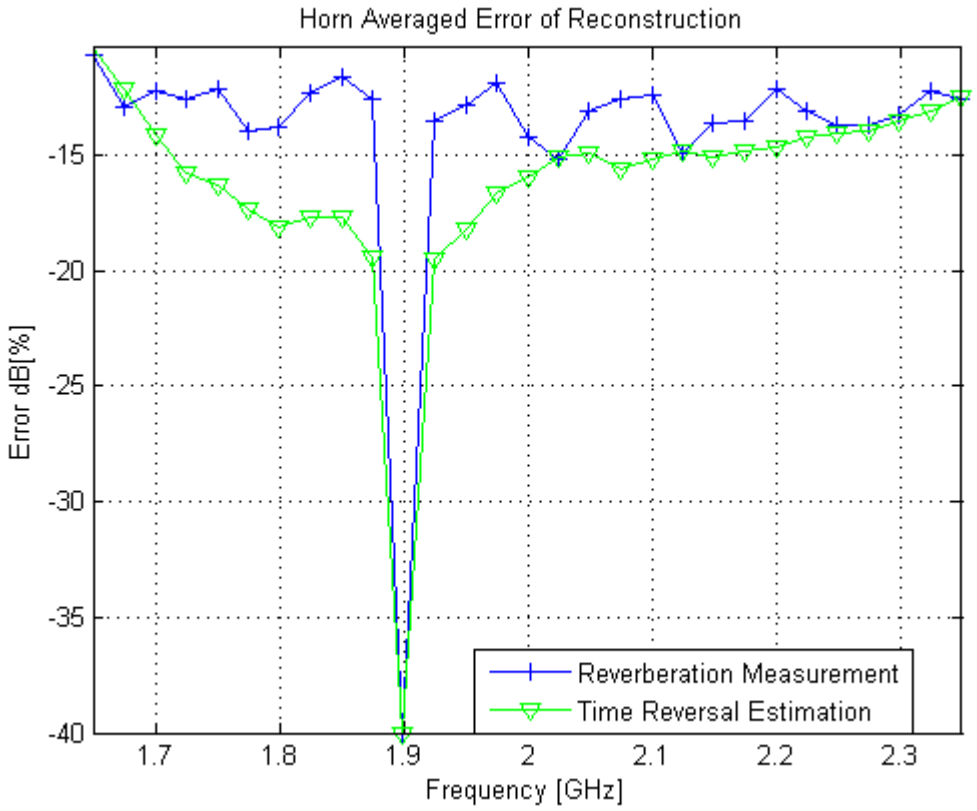


Fig. 25. Horn averaged normalized error (dB) versus frequency (Hz)

Afterwards, comparison is established using the average normalized error between antenna free-space radiation pattern estimation with Time Reversal technique and measurement in reverberation environment. Fig. 25 is averaged in VPA normalized error for Time Reversal technique first simulation. Fig. 25 is Horn AUT averaged normalized error where in the Time Reversal estimation error is lower than reverberation measurement in the frequency range from 1.7 GHz to 2.3 GHz.

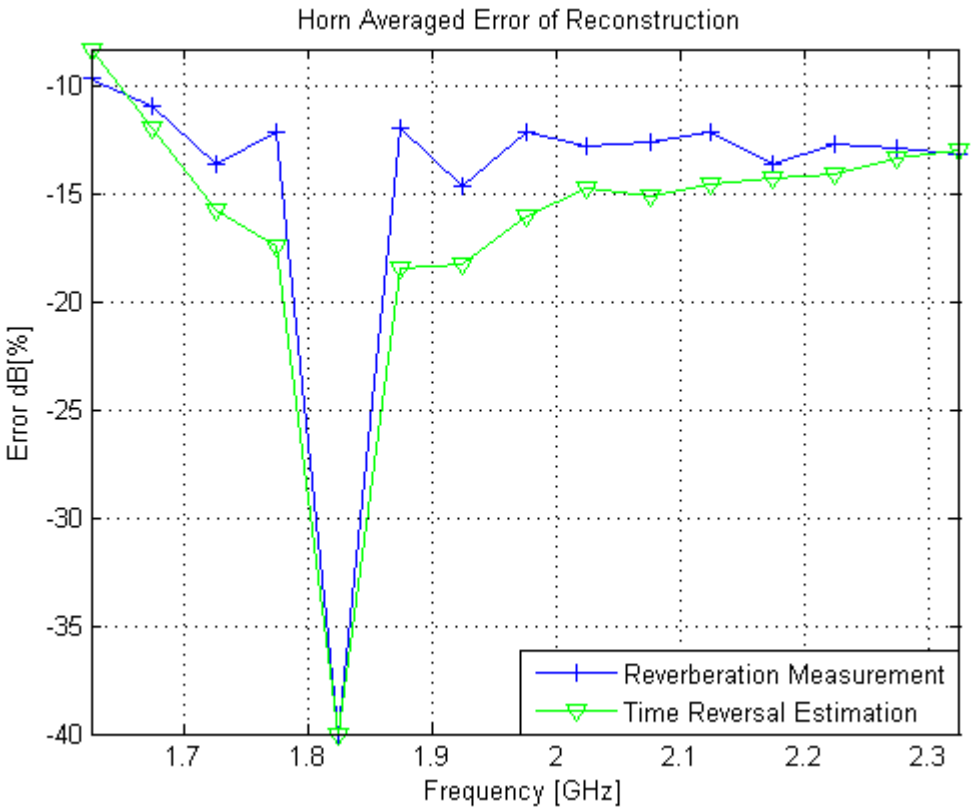


Fig. 26. Horn AUT Averaged normalized error in dB versus frequency for second simulation.

Fig. 26 is averaged normalized error for Time Reversal technique in second simulation. In Fig. 26, AUT Time Reversal estimation technique error is also lower than the reverberation measurement in the frequency range from 1.7 to 2.3 GHz.

Table IV provides indicators values or metrics to show performance of the antenna radiation pattern estimation using the Time Reversal algorithm for two simulations. Quantitative comparison of results uses average of the averaged normalized error, maximum standard deviation and Euclidean distance metrics to provide indicators of the accuracy of the antenna radiation pattern estimation performance for the Time Reversal technique in Table IV and Table V.

Table IV. Horn antenna radiation pattern Error of Estimation for first simulation.

| *Antenna* | *Measurement* \ *Error* | $E_{avg}$ | $\sigma_{\max}$ | Euclidean |
|---|---|---|---|---|
| Horn 1 VPA = 64, TRM = 20, Δf = 25 MHz | Reverberation measurement | 5.0% | 0.041 | 0.015 |
| | Time Reversal estimation | 3.16% | 0.042 | 0.0072 |

In Table IV. Horn antenna free-space radiation pattern estimation from 1.7 GHz to 2.3 GHz with Time Reversal technique performance is superior than the reverberation measurement according to

averaged normalized error and Euclidean distance, for maximum standard deviation the values are close.

Table V. Horn antenna radiation pattern Error of Estimation for second simulation.

| *Antenna* | *Measurement* \ *Error* | $E_{avg}$ | $\sigma_{\max}$ | *Euclidean* |
|---|---|---|---|---|
| Horn 2 VPA = 64, TRM = 20, Δf = 44 MHz | Reverberation measurement | 5.47% | 0.041 | 0.086 |
| | Time Reversal estimation | 3.92% | 0.055 | 0.0787 |

In Table V. Pyramidal Horn antenna free-space radiation pattern estimation from 1.7 GHz to 2.3 GHz with Time Reversal technique performance is superior than reverberation measurement in the same fashion as in the first simulation.

# V. CONCLUSIONS

Proposed Impulse Response method estimates the antenna 3D free-space radiation pattern fixing measurement in a single frequency and rotating the AUT orientation and elevation angular domain. Through qualitative and quantitative comparison the Impulse Response with 3D technique is a better option than Impulse Response with 2D technique. According to quantifiers the Impulse Response with 3D estimation provides higher accuracy, lower maximum standard deviation and shorter distance to the antenna free-space radiation pattern than the Impulse response with 2D estimation. Main contribution of this work is a robust reconstruction technique which may be employed as a tool in a multipath reflection environment because of the accurate characterization of vertically and horizontally oriented metallic objects disposition. Impulse Response with 3D technique can work in a reverberating environment where the metallic objects have combinations of azimuth and elevation orientations.

Time Reversal estimation quantifiers represent higher accuracy and shorter distance to the free-space radiation pattern than the reverberation measurements. Time Reversal accurate radiation pattern estimation depends of the adequate characterization of the Channel Matrix (CM). The CM depends of the number and orientation of half-wavelength dipoles in VPA, TRM and size of reflectors and can be used for different type of AUT measurements as long as all the remaining TREC conditions are not modified. Time Reversal

technique does not require the rotation of AUT and estimates the free-space radiation pattern in a frequency range up to 3 GHz. The Time Reversal technique should be used in complex reverberating environments

# REFERENCES

[1] Koh, J., De, A., Sarkar, T. K., Moon, S., Zhao, W. and Salazar-Palma, M. 2012. Free-Space Radiation Pattern Reconstruction from Non-anechoic Measurements Using an Impulse Response of the Environment. *IEEE Transactions on Antennas and Propagation*. Vol. 60, No. 2: 821-830.

[2] Bruns, C. and Vahldieck, R. 2005. A Closer Look at Reverberation Chamber – 3D Simulation and Experimental Verification. *IEEE Transactions On Electromagnetic Compatibility*. Vol. 47, No. 3: 616-626.

[3] IEC 61000-4-21. 2011. Electromagnetic Compatibility (EMC): Testing and measurements techniques. Reverberation chamber Test Methods. *International Electrotechnical Comission (IEC).* Part 4-21.

[4] IEC 61000-6-4:3006+AMD1:2010. 2011. Electromagnetic Compatibility (EMC) – Generic Standards – Emission Standard for Industrial Environments. Part 6-4.

[5] Loredo, S. and Pino, M. 2004. Echo Identification and Cancellation Techniques for Antenna Measurement in Non-anechoic Test Sites. *IEEE Antennas and Propagation Magazine.* Vol. 46, No. 1: 100-107.

[6] Black, D. and Joy, E. 1995. Test Zone Field Compensation. *IEEE Transactions on Antennas and Propagation.* Vol. 43, No. 4: 362-368.

[7] Toivanen, J. and Laitinen, T. Calibration of Multi-Probe Antenna Measurement System Using Test Zone Field Compensation.

*Department of Radio Science and Engineering, Helsinki University of Technology*.

[8] Pereira, J. and Anderson, A. 1984. New Procedure for Near-field Measurements of Microwave Antennas without Anechoic Environments. *IEE Proceedings.* Vol. 131, No. 6: 351-358.

[9] Fouristie, B. and Altman, Z. 1999. Anechoic Chamber Evaluation Using the Matrix Pencil Method. *IEEE Transactions on Electromagnetic Compatibility*. Vol. 41, No. 3: 169-174.

[10] Fouristie, B. and Altman, Z. 2001. Gabor Schemes for Analyzing Antenna Measurements. *IEEE Transactions on Antennas and Propagation*. Vol. 49, No. 9: 1245-1253.

[11] Cassereau, D. and Fink, M. 1992. Time-Reversal of Ultrasonic Fields – Part III: Theory of the Closed Time Reversal Cavity. *IEEE Transactions on Ultrasonics, Ferroelectrics, and Frequency Control.* Vol. 39, No. 5: 579-592.

[12] Maung, M. P. and Tun, H. M. 2014. Implementation of Acoustics based Time Reversal Mirrors for Source Localization. *International Journal of Scientific & Technology Research.* Vol. 3, No. 6: 265-269.

[13] Moussa, H. and Cozza, A. 2009. Directive Wavefronts Inside a Time Reversal Electromagnetic Chamber. *Department of Research in Electromagnetics. SUPELEC, IEEE International Symposium on Electromagnetic Compatibility: 159-164.*

[14] Choi, H. and Ogawa, Y. 2012. Angle and Time Domain Gating Technique for Time-Reversal Music Imaging. *Proceeding of ISAP,*

*Hokkaido University, Nagoya*. 86-89.

[15] Rasekh, P. and Razavian, M. 2015. Single-Antenna Time-Reversal Imaging Based on Independent Component Analysis. *Progress in Electromagnetics Research*. Vol. 44: 47-58.

[16] Ungureanu, A. and Fu, Y. 2011. Electromagnetic Source Synthesis by Reversed-TLM Method. *Microwave Symposium Digest, IMEP-LAHC Laboratory.*

[17] Cozza, A. and Moussa, H. 2009. Enforcing Deterministic Polarization in a Reverberating Environment. *Electronic Letters*. Vol. 45, No. 25.

[18] Chatelee, V. and Dubois A. 2007. Real Data Microwave Imaging and Time Reversal. *IEEE Antennas and Propagation Society International Symposium*. Laboratory of Electronic, Antennas and Telecommunication (LEAT), University of Nice-Sophia, France. 1793-1796.

[19] Zheng, W. and Zhao, Z. 2008. Application of TRM in the UWB through Wall Radar. *Progress in Electromagnetics Research, PIER 87.* 279-296.

[20] Bellomo, L. and Pioch, S. 2010. Time Reversal Experiments in the Microwave Range: Description of the Radar and Results. *Progress in Electromagnetics Research, PIER 104*. 427-448.

[21] Cozza, A. and el-Bassir, A. 2010. Accurate Radiation-Pattern Measurements in a Time-Reversal Electromagnetic Chamber. *Department of Research in Electromagnetics, SUPELEC. IEEE*

*Antennas and Propagation Magazine*. Vol. 52, No. 2: 186-193.

[22] Myong, R. 2015. Aircraft Survivability and Stealth Technology Lecture Note. *Department of Aerospace and Systems Engineering, Gyeongsang National University.* Chapter 6, EM Scattering and RCS Calculation: Scattering Mechanisms: 129-200.

[23] Mahafza, B. R. 2000, Radar Systems Analysis and Design using MATLAB. *Chapman and Hall/CRC*. Chapter 10, Radar Antennas: 339-368.

[24] Rahola, J. and Belloni, F. 2009. Modelling of Radiation Patterns Using Scalar Spherical Harmonics with Vector Coefficients. *3rd European Conference on Antennas and Propagation*. 3361-3365.

[25] Yang, J., Pivnenko, S., Carlsson, T. J. and Chen, X. 2010. Measurements of Diversity Gain and Radiation Efficiency of the Eleven Antenna by using Different Measurement Techniques. *Proceedings of the the Fourth European Conference on Antennas and Propagation*. 1-5.

[26] Chen, X., Kildal, P. and Carlsson, J. 2011.Comparisons of Different Methods to Determine Correlation Applied to Multi-port UWB Eleven Antenna, *5TH European Conference on Antennas and Propagation.* 1776-1780.

[27] Punnoose, J. and Counsil, D. 2011. Time Reversal Signal Processing for Communication. *Sandia report SAND2011-7050, Sandia National Laboratories*. 1-48.

[28] Kolundzija, B., Ognjanovic, J., Sarkar, T. K., Tasic, M., Olcan, B. and Sumic, D. 2004. WIPL-D Pro V5.1. 2004. *Electromagnetic Modeling of Composite Metallic and Dielectric Structures. 3D Electromagnetic Solver Professional Edition. WIPL-D Ltd.* User's Manual Introduction, What is WIPL-D?: 1-1:1-2.